8-2010

Diffuse Ultrasonic Scattering in Advanced Composites

Christer Stenström
University of Nebraska-Lincoln, christer.stenstrom@gmail.com

Diffuse Ultrasonic Scattering in Advanced Composites

by

Christer Stenström

A THESIS

Presented to the Faculty of
The Graduate College at the University of Nebraska
In Partial Fulfillment of Requirements
For the Degree of Master of Science

Major: Engineering Mechanics

Under the Supervision of
Joseph A. Turner
and
Janis Varna

Lincoln, Nebraska

August, 2010

Diffuse Ultrasonic Scattering in Advanced Composites

Christer Stenström, M.S.

University of Nebraska, 2010

Advisers: Joseph A. Turner and Janis Varna

Non destructive testing (NDT) is a noninvasive technique used for characterization and inspection of the integrity of objects. NDT is an important tool for research, manufacturing monitoring and in-service inspections. Ultrasonic testing is the most used NDT technique, which for advanced composites can identify several types of defects, like delamination and interlaminar cracks. Diffuse ultrasonics has shown to be able to extract information at the microscale of metals and therefore it is believed it can be used for advanced composites to extract microstructural information, i.e. at the level of fibers.

In this thesis, diffuse ultrasonic methods, together with spatial variance analysis, have been used to quantify the scattering within unidirectional advanced composites that have been loaded to different states of fiber damage.

Results show that the spread in data is too large to give a clear trend of how the scattering changes with fiber damage. Further research has to be done in order to lower the spread in the results and increase the reproducibility. This can be done with higher precision in the experimental set-ups and new parametric analysis.

Acknowledgements

This work was possible thanks to the EMME Programme: EU-US Transatlantic Degree Program in Engineering Mechanics/Materials Engineering, which is a project within the EU-US Atlantis Programme. The EMME Programme is a collaboration between the University of Nebraska - Lincoln (UNL), Université de Rouen (UR) and Luleå University of Technology (LTU) funded by European Commission and US Department of Education. Thank you all and thank you Erasmus Programme and Erasmus Mundus for providing with scholarships.

I would like to thank my UNL advisor Dr. Joseph A. Turner for his guidance and support throughout my year abroad in Lincoln. I would like to extend my thanks to my LTU advisor Dr. Janis Varna and the LTU Director of Graduate programs Dr. Lennart Wallström for making my year abroad possible. I would like to thank my committee members Dr. David H. Allen, the UNL Director of Graduate programs Dr. Mehrdad Negahban and once again Dr. Joseph A. Turner. I also would like to thank my fellow graduate students for their support and assistance.

Finally, I would like to thank my daughter, my wife and my parents for always being there, supporting and understanding.

Contents

List of Figures

List of Tables

Chapter 1

Introduction

Non destructive testing (NDT) refers to noninvasive techniques used for characterization and inspection of objects. Important fields are aerospace, automotive, marine, nuclear and wind turbines [1]. Also industries in the fields of circuit boards, pipes and sport goods, among others, have an interest in such techniques [1]. NDT is used for research, manufacturing monitoring and in-service inspections to extract information of a material's integrity.

Advanced composites possess anisotropy, heterogeneity, often multiple plies and a matrix that gives arise to viscoelastic losses. Therefore NDT is complicated in this kind of material. Also the statistical dispersion of the properties is higher in advanced composite materials than for metals. The manufacturing method is crucial for minimizing the statistical dispersion. NDT can be used to measure the statistical dispersion, but at the same time this dispersion can make the NDT more complicated.

There are many NDT methods that can be used on advanced composites. Ultra-

sonic testing (UT) is the most used method followed by radiography and thermography. Ultrasonic testing can be used to detect many kinds of different flaws and damage in advanced composites. Some properties and damage can be measured directly whereas some must be measured indirectly [2]. Ultrasonic testing is extensively used with satisfying results in materials at a level where the material can be seen as homogeneous. For wave lengths close to the length scale of the heterogeneity of the material the resolution and detectability is limited. As a rule of thumb, the size of a discontinuity has to be at least half the wave length that one is using in order to be detectable by conventional ultrasonic testing. Diffuse ultrasonics is the study of diffuse scattering, defined by random scattering in all directions (Figure 1.1). By studying diffuse ultrasonics it is possible to extract irregularities close to the scale of heterogeneity. The heterogeneity gives rise to multiple scattering and attenuation of the ultrasonic wave and therefore testing close to heterogeneity, e.g. grain size or fiber diameter, of these materials is a challenge. The multiple scattering effects also give rise to an effective noise where the information one is trying to extract can be hidden. Diffuse ultrasonic scattering together with spatial variance calculations have shown to be useful for investigating the microstructure of steel and concrete [3, 24]. Ghoshal and Turner derived a theoretical model for diffuse ultrasonic scattering and fit it to spatial variance curves from experiments on steels with good agreement [3, 25, 26]. Experimentally, diffuse ultrasonics, utilizes the spatial variance of the signal to extract information about the microstructure. By calculating the variance of a virgin sample one receives a reference curve that is characteristic of the material. By comparing this reference variance curve to a damaged sample of the same kind

of material one can see material changes at the level of heterogeneity. This approach is used in this thesis on advanced composite materials to give a measure of fiber breakage in unidirectional composites.

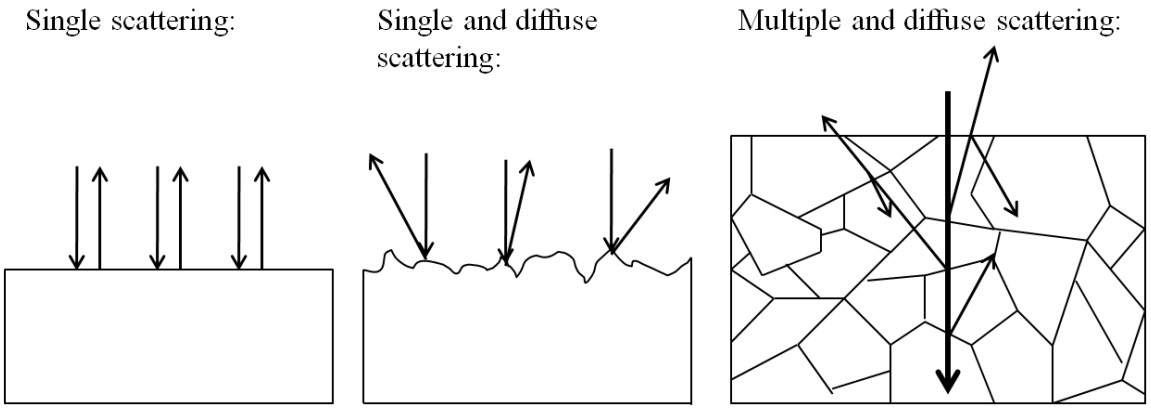

Figure 1.1: Different kinds of scattering. From left to right: single scattering, single and diffuse scattering, and multiple and diffuse scattering.

The variance is defined by:

$$var[V_M(t)] = < V_M(t)^2 > - < V_M(t) >^2, \tag{1.1}$$

where M is the number of acquired signals, i.e. the number of scan points, and <> stands for the mean value.

In the next section, the most common NDT methods for advanced composites are briefly described. The subsequent section is dedicated to ultrasonic testing only as applied to advanced composites.

1.1 Non Destructive Testing of Advanced Composites

Since the 1960s the use of carbon fibers and other high performing fibers have increased steadily with technology and lower price. The request for rapid and capable NDT methods has increased at the same time. Advanced composites are used for their high specific stiffness and specific strength, which is requested either for high performance or for economical benefits. It is the same reason that makes NDT important, hand in hand with safety.

The most used NDT methods are ultrasonic testing, radiography and thermography. Radiography is the use of an x-ray beam crossing through a object and taken up by a film or detector. The x-ray beam attenuates depending on the spatial density variation within the object, which is the basis of the received image. Radiography is more sensitive than UT to find transverse cracks, but on the other hand, planar defects perpendicular to the x-ray source can go undetected [1, 4]. Radiography needs two sided access, it is hazardous and an infiltrant is often needed. With ultra high resolution computed tomography (3D representation by sectioning) it is possible to identify single fiber breaks [5]. But this is an expensive and time consuming method and therefore it is interesting to find another method which is able to measure fiber breakage.

Thermography is another method that is used in many industries. A heat pulse is applied to the surface of an object to raise the temperature by a few degrees. The heat dispersion and radiation at the surface is affected by anomalies near the surface. An image is constucted by the use of a thermograpic camera. It is less capable method to detect small discontinities but it is rapid and easy to interpret [1, 6].

1.2 Ultrasonic Testing of Advanced Composites

Ultrasonic testing has high resolution, good penetration depth, one and two-sided set-up possibilities and it is nonhazardous. The main drawbacks are its line-by-line scan which makes it relatievly slow compared to some other NDT methods. In addition ultrasonic inspection usually requires an experienced operator. Nevertheless, it is a capable technique.

Ultrasonic testing can be operated manually or the testing can be automated. A system for manual testing consists of a pulser/receiver, a transducer and an oscilloscope. An automated controlled system consists of the same components but the transducer is controlled by a mechanism that moves in several axes. Ultrasonic methods work by the pulser/receiver (P/R) sending pulses of electric energy to a transducer. The transducer's main component, a piezo-electric material, transforms the electric energy into mechanical strain and generates a material displacement pulse, i.e. a sound wave. Changes in acoustic impedance in the wave's path results in reflections. The reflections or what is left of the signal is then taken up by the same or another transducer and processed by the pulser/receiver. The result can then be seen on an oscilloscope (Figure 1.2).

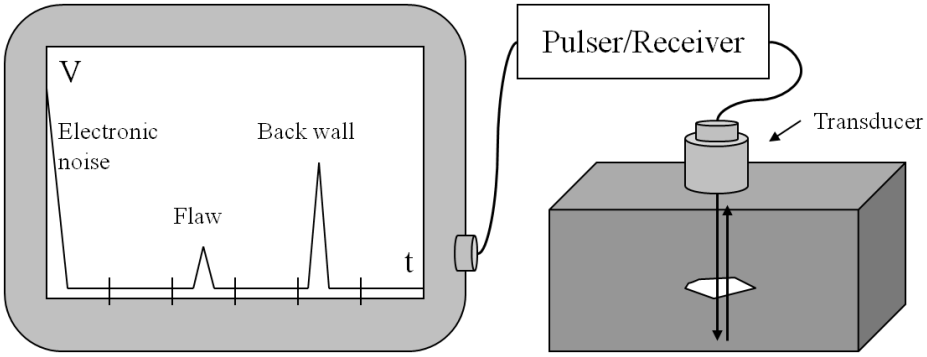

Figure 1.2: Hand held contact in an echo set-up, giving an A-scan.

Transducers are available both for air coupling and for coupling by using a liquid. The acoustic impedance difference between air and a solid is very large and therefore a small amount of ultrasound energy is transmitted through each interface the wave meets. A liquid, such as water, has an acoustic impedance closer to a solid and therefore most ultrasonic testing is done with liquid coupling. There are two kinds of transducers for liquid coupling, contact transducers and immersion transducers. In a manual test one often uses a contact transducer together with an oil or semisolid couplant and in an automated system one uses a water immersion tank or a water squirting system.

Ultrasonic testing can be set-up in a pulse echo mode or in a through transmission mode. In a pulse echo set-up one can see echoes resulting from reflections from the front and back wall (Figure 1.2). In a through-transmission set-up the first acquired signal will have passed the material one time, the second will have passed the material three times, and so on. Therefore all acquired signals will have information of both the front and the back wall (Figure 1.3).

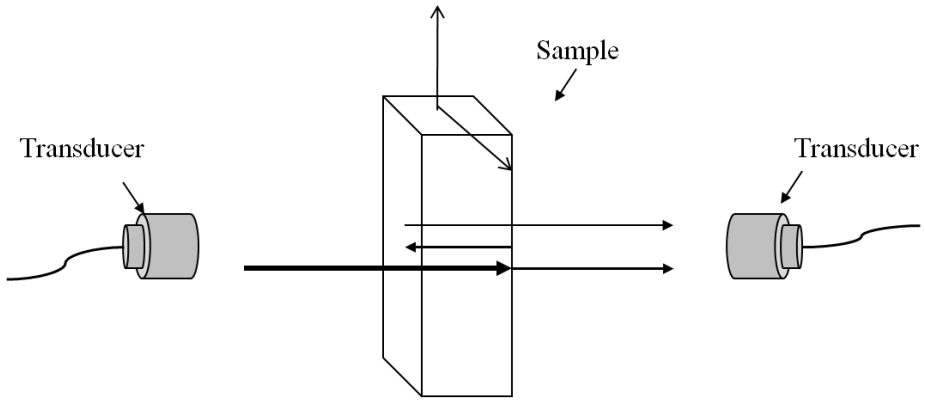

Figure 1.3: Automated immersion testing in through transmission set-up, giving a C-scan.

The most common images constructed are A-scan, B-scan, and C-scan. An A-scan (Amplitude scan) gives a one dimensional view of the received signal (Figure 1.2), a B-scan (Brightness scan) gives a two dimensional cross-sectional view, and a C-scan (Compound scan) gives a planar view (Figure 1.4). The C-scan is constructed by assembling many A-scans taken line-by-line over an area of points by using an automated system. At each spatial point the average of a number of scans is taken in order to reduce the noise. The spatial variance is found by carrying out a C-scan and calculating the variance of the A-scans from all the scan points. How many scan points to use for the variance has to be decided. If too few points are used the varaince can be affected by a local anomalie, but in the other hand if too many points are used the variance can be effected by alignment and leveling in the experimental set-up.

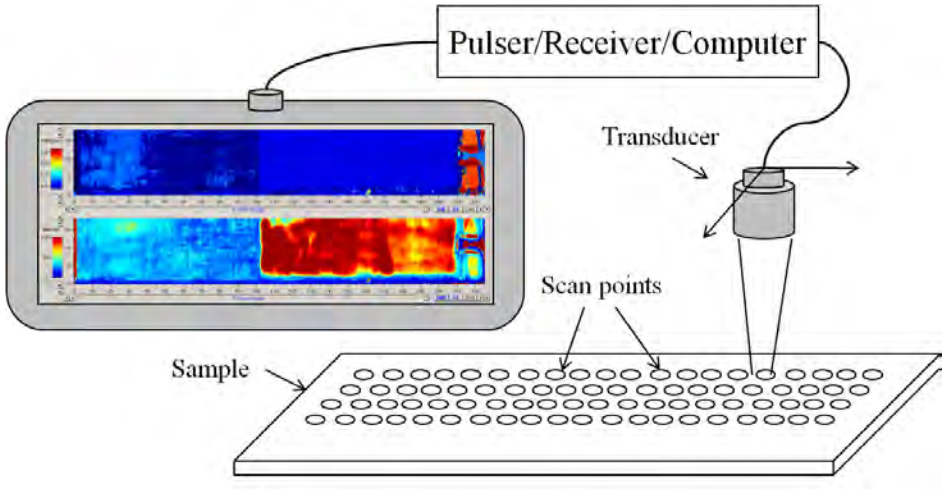

Figure 1.4: Automated immersion testing in echo set-up, giving a C-scan.

Both normal and oblique incidence of the ultrasonic wave are used in ultrasonic testing. If an oblique incidence is used, a mode conversion will occur and there will be portions of longitudinal and transverse waves (shear waves) within the material. This conversion phenomenon has several advantages. The energy transfer is more efficient in steel and similar materials, the wavelength is shorter than for longitudinal wave at a given frequency and some defects are easier to detect, e.g. interlaminar cracks. Shear waves are discussed more in Chapter 3.

1.3 The Structure of Advanced Composites

Advanced composites are composed of high performing long fibers in a thermosetting matrix, usually epoxy. Thermoplastics as a resin is uncommon, but the market is growing due to their recyclability. A laminate is built up by unidirectional transversely isotropic plies. In most cases, a symmetric and quasi-isotropic lay-up is desired to avoid warping and to have an isotropic material in one plane. A quasi-

isotropic laminate is achived if the number of plies $N \geq 3$ with equal change in angle between adjacent plies, $\Delta\theta = \pi/N$. Unidirectional laminates are commonly used in research because they are easy to work with. Composites are heterogeneous since there never exist perfect ordering of the fibers. A schematic of an unidirectional composite can be seen in Figure 1.5.

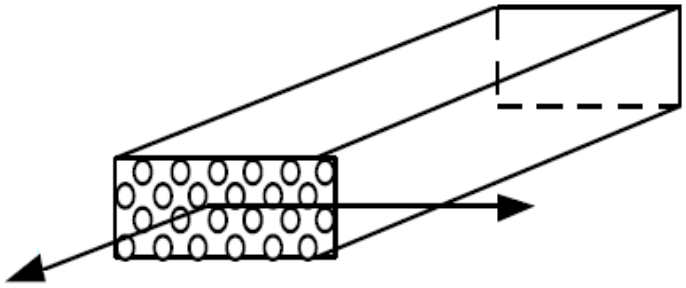

Figure 1.5: A schematic of an unidirectional composite.

1.4 Flaws and Damage in Advanced Composites

Flaws and damage appear both in manufacturing and in-service. Imperfect manufacturing can result in poor curing, cracks, poor interlaminar bond, porosity, inclusions, ply waviness, errors in orientation and errors in lay-up sequence [7]. Poor curing and interlaminar bonds can come from using cure temperature that is too low or from a curing time that is too short. If the curing temperature is too high it can result in transverse cracks. Errors in lay-up sequence or orientation of plies can give severe changes to global properties. Ply waviness lowers the initial stiffness and increases matrix stresses. Porosity is defined as the concentration of microvoids. Microvoids tend to concentrate at resin rich areas, such as the ply interfaces, which affect the shear strength [2, 8].

Sandwiched honeycomb structures, which are materials in a honeycomb geometry between two facesheets for high bending stiffness, can suffer from similar defects and damage, but here the bond between the facesheet and the core has to be inspected as well. This can be done by using squirters in a through transmission set-up [7].

In-service damage can arise from the outside environment or from underlying imperfect manufacturing. Impact damage is the most common in-service problem in composites, resulting in delamination and microcracking of the matrix [27].

Some damage can be measured directly by ultrasonic testing, while others have to be measured indirectly. Porosity and fiber volume fraction are often estimated by the use of attenuation [2]. Diffuse ultrasonics give a measure of the amount of scattering inside a material. Compared to using attenuation it is a more direct way of measuring scattering and therefore has the potential to be more exact.

1.5 Purpose

The purpose of this thesis is to investigate whether or not diffuse ultrasonic testing with spatial variance analysis can be used on advanced composites to give a measure of fiber breakage. If it is shown to be possible it can be valuable in further research, e.g. in micro mechanics. Several instrumental set-ups and two kinds of materials have been used for this study.

1.6 Objectives

The specific objectives of this research work are to:

- Perform a parametric study of important variables for the spatial variance analysis, i.e. the number of signals to acquire and the angle of incidence.
- Set-up and complete suitable diffuse ultrasonic scattering experiments for unidirectional advanced composites.

1.7 Outline of Thesis

In the next chapter, previous work on ultrasonic testing of advanced composites and diffuse scattering is reviewed. In Chapter 3 the chosen materials, the experimental set-ups and the theory are discussed. Also the two parametric analyses are carried out. Chaper 4 is decicated to present the results and in Chapter 5 discussion and concluding remarks are found. There are also two appendices attached to the thesis. Conventional ultrasonic testing is described in Appendix A, which is a good start for the unfamiliar reader. In Appendix B a description and a collection of photographs of the experimental equipment are found.

Chapter 2

Background

With the development of advanced composites in 1960-70s and their introduction in critical structures, new ultrasonic testing methods were required, and still are. The first research papers on advanced composites were mainly focused on extracting the elastic constants and the wave speeds [9, 10, 11, 12, 13]. Around the same time, studies on the attenuation versus frequency, void content and damage state were carried out [14, 15, 16]. Also several instruments with pulse-echo A-scan and fundamental frequency monitoring possibilities were developed for industry, e.g. Ultrasonoscope, Novascope 2000, Fokker Bondtester and 210 Bondtester [16, 17, 18]. In the 1980s automated scanning systems, i.e. C-scan capable systems, were commercially available with video monitoring, e.g. the McDonnell AUSS with ultrasonic frequencies up to 10 MHz [18]. At this time it was possible to recognize anomalies such as delamination, voids, resin rich and starved areas. Researchers tried to identify interlaminar cracks by studying the attenuation but it was hard to distinguish them from voids [16].

With new methods and more sophisticated equipment new research on interlaminar cracks was performed in the 1990s [4, 19, 20, 21, 22, 23]. By using a spherically focused transducer with a central frequency of 15 MHz, Gorman was able to show transverse cracks in CFRP cross-ply with the use of a polar backscattering set-up in echo mode [19]. The lay-up was a $[0,90]_s$ made of IM6/3501-6 pre-pregs with a ply-thickness of 140 μm. The angle of incidence used was 27°, but the result was not sensitive to a change in angle of ± 2°. The received singal was only scattering, i.e. no front or back wall could be onserved. Kinra et al used the same technique for ply-by-ply detection of interlaminar cracks on liquid hydrogen treated $[90/45/0/-45]_s$ laminates [20]. It is not mentioned what kind of material or what the composition was but it was provided by NASA for research on the reusable launch vehicle so it is most likely a high performing CFRP with thin plies. With the proper gate setting they were able to show interlaminar cracks for each ply with a 20 MHz transducer at 25° angle of incidence. However, experimental details were not provided. Maslov used an inclined through-transmission technique to show transverse cracks with an 18 MHz cylindrically focused transducer at 30° angle of incidence [21]. The material was carbon fibers in a bis-maleimides matrix (CF/BMI) with a ply-thickness of 130 μm.

If interlaminar crack faces are close to each other, so called kissing bonds, the cracks can be invisible for compressional waves but seen by Lamb waves (a group of in-plane waves) and shear waves and therefore set-ups with oblique sonification are favorable [22, 23]. If there are sufficient residual stresses so the cracks have an opening it is possible to detect them with perpendicular C-scan [4]. One can assume

that the same principle is true for broken fibers but an opening between the crack faces is even less likely to appear due to residual stesses. The large difference in thermal expansion coefficient and the elevated curing temperature puts the matrix in tension and the fibers in compression at room temperature. If this residual stress has some effect on the fiber crack openings it is not clear since the strength and stiffness difference is so large. At least, there is nothing that promotes an opening of fiber cracks, beside the possibility of some internal stresses in the fibers from the fiber production.

The research above shows that inclined through-transmission works for detection of transverse cracks and therefore an inclined set-up can be a reasonable choice for measuring scattering from fiber breakage. On this basis inclined sonification was chosen for the experiments in this thesis.

Diffuse ultrasonic scattering together with variance calculations have shown to be useful for investigating the microstructure of steel and concrete [3, 24]. Ghoshal and Turner derived a theoretical model for diffuse ultrasonic scattering and fit it to variance curves from experiments on steels with good agreement [3, 25, 26]. The diffuse scattering arises from the grains within the steel and therefore this method is useful to extract microstructural information. In one of the experiments by Ghoshal and Turner, a 15 MHz transducer was used for studying the scattering within steel. With a longitudinal speed of 6000 m/s one receives a wavelength of 400 μm. From a micrograph the mean grain size was found to be 15.5 μm. This value was comfirmed by the theroretical model with a deviation of 1.3 %. These results gave the idea to use the same approach to measure fiber breakage in advanced composites.

Chapter 3

Material and Method

This chapter is devoted to the materials used, the experimantal set-ups and also the parametric experiments, which are presented with conclusions.

3.1 Material

In this thesis two different materials have been used, carbon fiber reinforced plastics (CFRP) and glass fiber reinforced plastics (GFRP), both with unidirectional lay-ups. Glass fiber is not considered as an advanced material but it was chosen because of its larger fiber diameter in comparison with carbon fiber and therefore it is interesting as a comparison.

The carbon fiber material is supplied by McMaster-Carr Supply Company. The material composition and the material manufacturer are proprietary information and therefore microscopical study and energy-dispersive x-ray spectroscopy (EDS) had to be carried out. Samples were prepared by grinding and polishing with diamond

slurry down to 3 μm. Microscopical image and x-ray energy spectrum can be seen in Figures 3.1-2. The fiber diameter is found to be 7.0 μm by averaging several fiber diameters, which were found by pixel comaparison of a microscope scale. The peak on the left hand side of Figure 3.2 in x-ray energy spectrum corresponds to the discrete energy levels of carbon. The fibers are therefore carbon fibers.

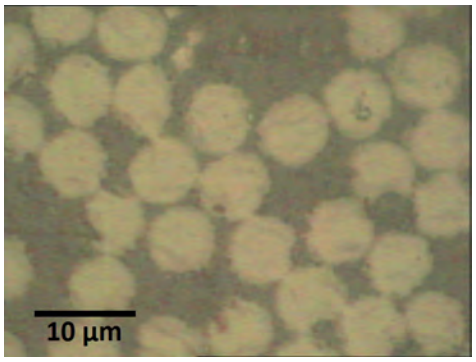

Figure 3.1: Microscopical image of the cross-section of the CFRP material showing the fibers.

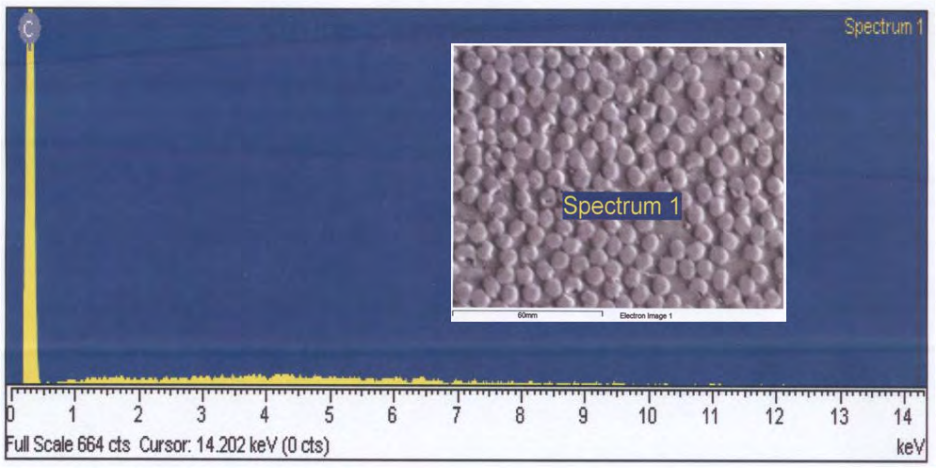

Figure 3.2: X-ray energy spectrum of a singel carbon fiber.

The GFRP is manufactured by Gordon Composites. Most of the physical and mechanical properties are known and given in Table 3.1, with the exception of the fiber diameter and matrix material. The sample preparation and microscopical

measurement was done in the same way as for the CFRP sample. The fiber diameter is found to be 16.5 μm, Figure 3.3.

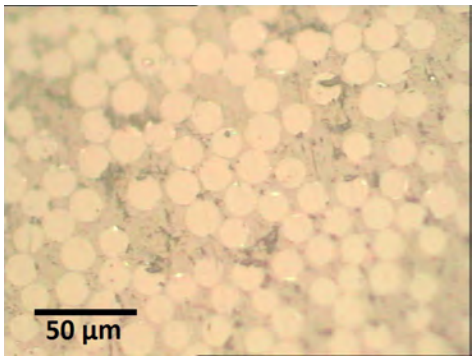

Figure 3.3: Microscopical image of GFRP material.

The matrix of the composite material is unknown but assumed to be a thermoset since thermoplastics in advanced materials are uncommon. Therefore the matrices are assumed to be epoxy, unsaturated polyester or vinylester. Because of the thermoset assumption the ultrasonic speed is assumed to be similar.

The longitudinal tensile strength had to be determined to be able to load the samples to certain percentages of their strength to achieve different states of damage. An Instron 8500 Plus was used for this purpose. The Instron was set to strain control with a slope of $3 - 5 \cdot 10^{-4}\ s^{-1}$ (strain/time), which corresponded to a loading time of 2 - 4 min. The tensile test curves can be seen in Figure 3.4. The mean longitudinal tensile strength was calculated from five samples, which were tensile tested to breakage. The mean tensile strength of the CFRP samples is 1870 MPa with maximum of 2110 MPa and minimum of 1610 MPa. For the GFRP samples the mean tensile strength is 1270 MPa with maximum of 1310 MPa and minimum of 1208 MPa. The strength of the material and some other important properties for this research are

found in Table 3.1, where the star indicates values taken from the manufacturer data sheet.

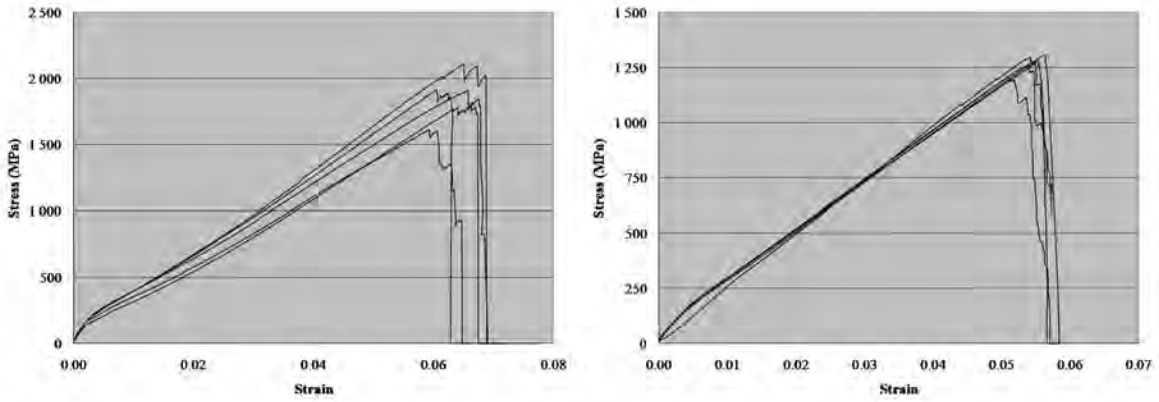

Figure 3.4: Tensile test curves: Left: CFRP, Right: GFRP.

Table 3.1: Material properties of the CFRP and GFRP. * indicates values taken from the manufacturer data sheet.

	CFRP	**GFRP**
V_f (wt. %)	Unknown	70*
Fiber $\varnothing$ (μm)	7.0	16.5
Density (kg/m^3)	Unknown	1880*
Mean Tensile Strength (MPa)	1870	1270
Matrix Material	Unknown	Unknown

The CFRP samples are made from a bar with a cross-section of 1.78 x 11.1 mm, which is the cross-section of the final CFRP samples. For the GFRP samples the raw material was a sheet. After cutting, the final cross-section was 1.18 x 13.6 mm. These dimensions can be compared with the transducers focal diameter which is between 10-13 mm. The length of all samples is in the range of 20-25 cm. Glass fiber reinforced tabs were glued to the samples with high shear strength and slow curing epoxi. Photographs of the samples are given in Appendix B.

When the thicknesses of the two materials and the wave speed are known one can calculate the theoretical time of flight (TOF) between the front and back wall. The thicknesses of 1.78 and 1.18 mm and a longitudinal wave speed in the transverse direction of 3000 m/s gives a time of flight (TOF) between front and back wall of 1.2 and 0.8 μs, respectively. Using a wave speed of 3000 m/s is close to the measured value in Appendix A, Table A.2, and it is useable for both CFRP and GFRP since the transverse wave speed and the matrices is assumed to be similar in both materials. The theoretical time of flight 1.2 and 0.8 μs can be compared with the measured in Figure 3.5, where one can see the TOF between the front and back wall. The two graphs in the figure are different because one of them is from the signal acquiring software and the other one is from data transfered to another software. The set-up is in perpendicular echo mode. A frequency of 15 MHz was used for the left graph and a frequency of 20 MHz was used for the right graph. Knowing theoretically where the back wall is and by making experiments at lower frequencies is practical when higher frequencies are used where the attenuation makes the back wall hard to see.

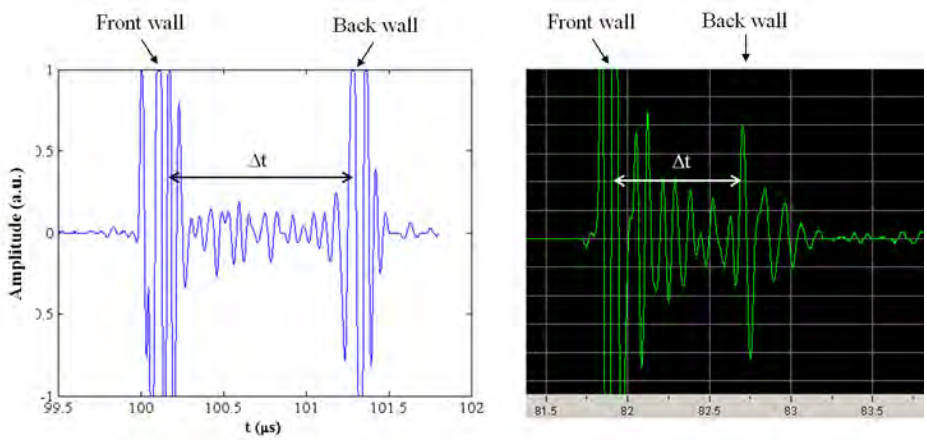

Figure 3.5: Perpendicular A-scan of CFRP and GFRP with 15 and 20 MHz transducer, respectively. The front wall, back wall and the TOF is seen.

3.2 Experimental Set-up

The immersion system is an ULTRAPAC^{TM} system from NDT Automation, using UTWin software, together with an DPR300 pulser/receiver (P/R) from JSR Ultrasonics, Figure 3.6 (details are given in Appendix B).

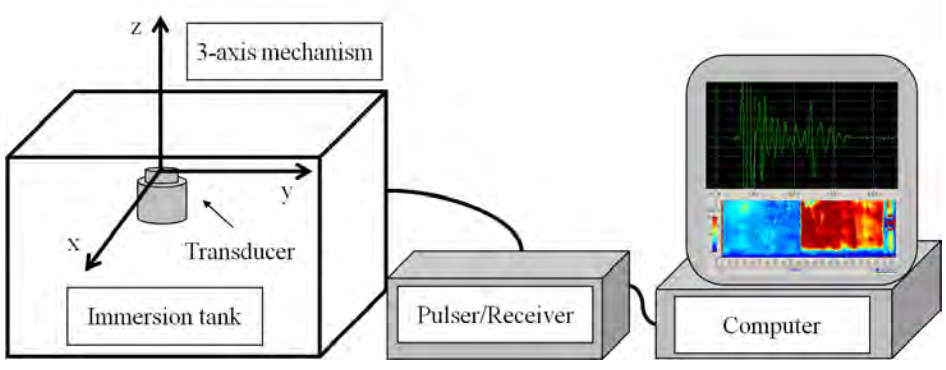

Figure 3.6: A schematic of the ultrasonic testing system.

The transducers are spherically focused and manufactured by Olympus Panametrics with a frequency of 15-25 MHz. The focusing distance is 3.0″ which in water

takes approximately 100 μs to travel. The speed of ultrasound in water is 1.48 mm/μs. A common method for studying the ultrasonic response is to use a glass sample. A glass sample is choosen because it has a smooth surface and it is amorphous, i.e. non-crystalline, and therefore scattering within the material is minimal. In Figure 3.7 one can see the response from a glass surface with a 15 MHz transducer in an echo set-up. If one would like to determine the spatial position of an obstacle one sees from this figure that the exactness in the result depends on the pulse width. See Table 3.2 for P/R settings.

Table 3.2: Experimental set-up and settings for glass response experiment.

Experimental set-up	⊥ echo
Transducer freq. (MHz)	15
Rel. Gain (dB)	25
Pulse Amp.	9
Pulse Energy	1 low z
Damping	9

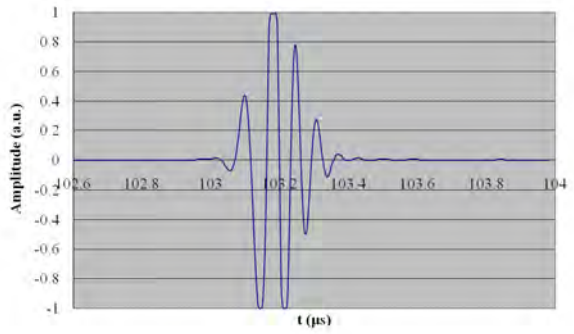

Figure 3.7: Glass surface response showing the wave width from a 15 MHz transducer in a echo set-up.

Two fixtures were designed for the experiments, one fixture for the transducers and one for the samples. Fixtures in an inclined set-up can be seen in Figure 3.8.

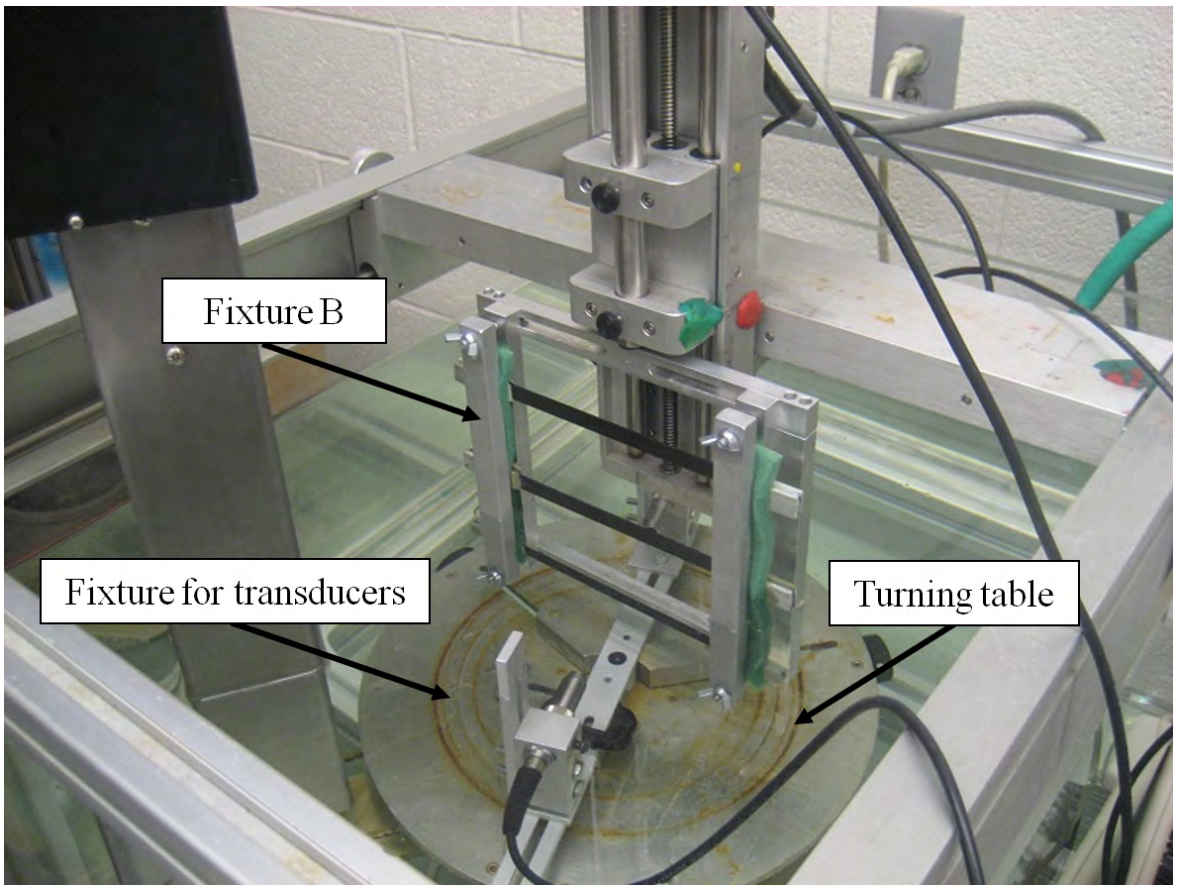

Figure 3.8: Immersion tank and fixtures in an inclined set-up.

3.3 Theory and Method

On the basis of the discussion in the Background, diffuse ultrasonics with spatial variance calculations are found to be an interesting technique to use on advanced composite to measure scattering from fiber breakage. The variance is a measure of the spread in a set of data. For a random variable the variance can be expressed in the following way:

$$var[V_M(t)] = < V_M(t)^2 > - < V_M(t) >^2, \tag{3.1}$$

where M is the number of acquired signals, i.e. the number of scan points, and <> stands for the mean value. The variance has the property that if all data points in a set of data have the same value, then there is no variance, and vice versa. This phenomenon can be seen in Figure 3.9. The figure shows one of the 100 acquired signals and the variance of all the 100 acquired signals. In the top left graph one sees that the acquired signals amplitude equals one as a result of the high gain. In the bottom right graph one sees that the corresponding variance is close to zero when the signal response is one. See Table 3.3 for P/R settings and experimental set-up.

Table 3.3: Experimental set-up and P/R settings for studying the variance.

Experimental set-up	⊥ echo
Material used	CFRP
Transducer freq. (MHz)	25
Rel. Gain (dB)	55
Pulse Amp.	9
Pulse Energy	1 low z
Damping	9

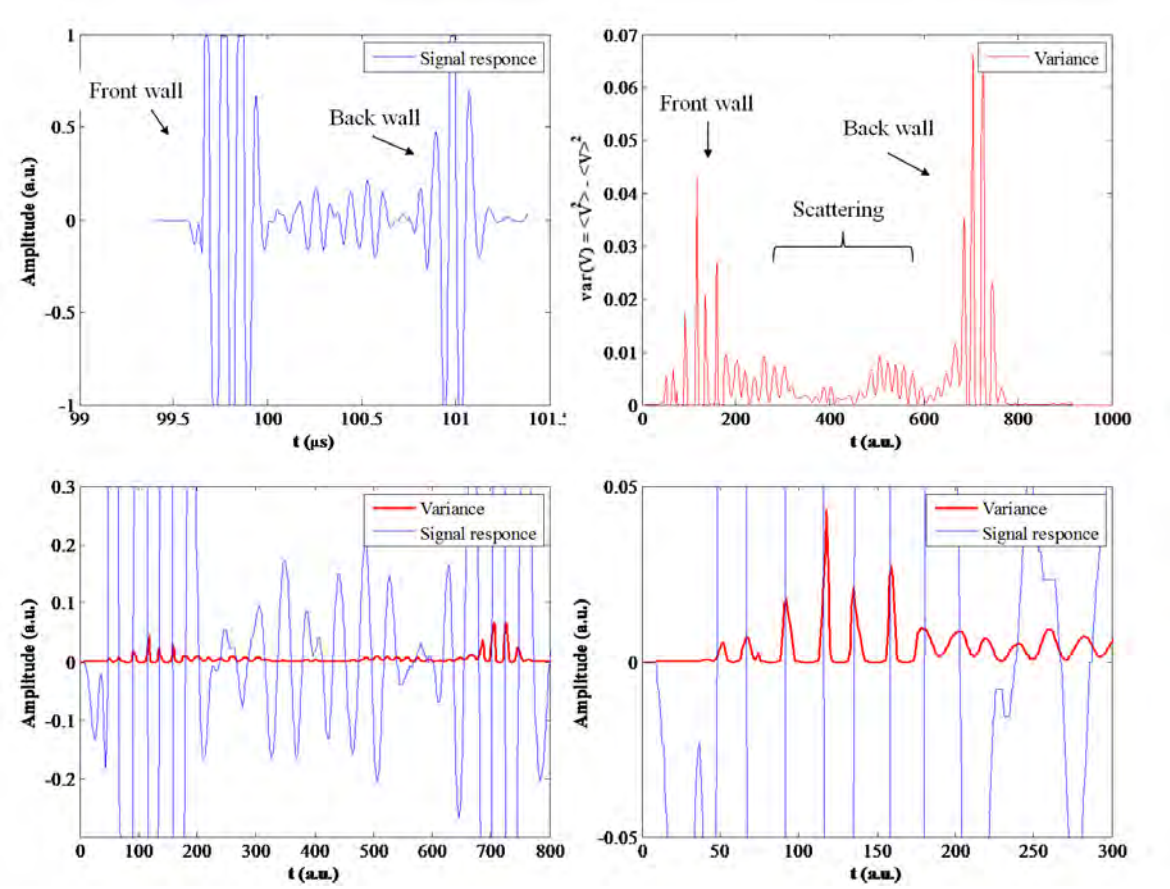

Figure 3.9: Top left graph: One of the 100 acquired signals. Top right graph: The variance of 100 signals. Bottom graphs: The above graphs plotted on each other.

Scattering within a material is random in random directions. If there exist scattering, it can be visualized and measured by calculating the variance over a number of points M, see Figure 3.9, 3.11 and 3.12, where the scattering is identified. The number of scan points M has to be determined in order to receive a variance affected as little as possible by local anomalies and unperfect alignment and leveling.

3.3.1 Calculating the Variance

By calculating the variance over an area of points of a material one receives a unique profile of the material with its scattering. An experimental set-up can never be

perfect in level and alignment, and therefore there will be differences in the time of flight of the ultrasonic wave when a scan over a surface is done. This problem can be worked out by shifting each acquired signal. The drawback is that the variance will be small at the point where the shift is done since the fit of the signals will be locally very good. Therefore shifting each signal at the frontwall can make the frontwall disappear, depending on the set-up and P/R settings. See Figures 3.10-11 and Figure 3.9 above. The results in Figure 3.10-11 comes from a 1.2 mm thick CFRP made of T700 Toray fibers and an epoxy matrix. In Figure 3.10 one can see all signals before and after the shift from a 2x2 mm scan with the resolution 200 μm, i.e. 100 signals. In the right plot it can be seen that the shift is done where the curve comes from the first local minima and crosses the x-axis. The resulting variances are found in Figure 3.11, where the front wall is barely visible. In Figure 3.9 the same type of shifting is done but here the front wall is visible due to higher gain making the signal response go above one (top left of Figure 3.9).

In all the following experiments, where it is possible to make a shift, it is done in this way. The resolution is 200 μm throughout the whole thesis, i.e. the distance between scan points.

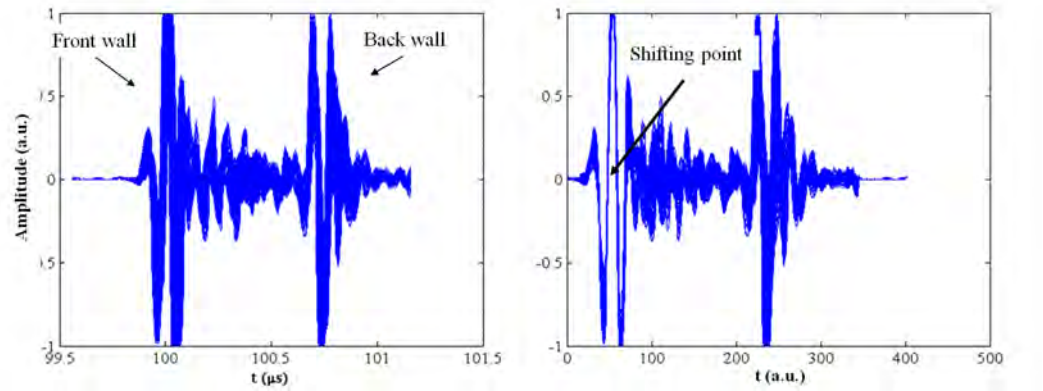

Figure 3.10: 100 signals from 100 scan points. Left: No shift, Right: Shifted to the labeled point.

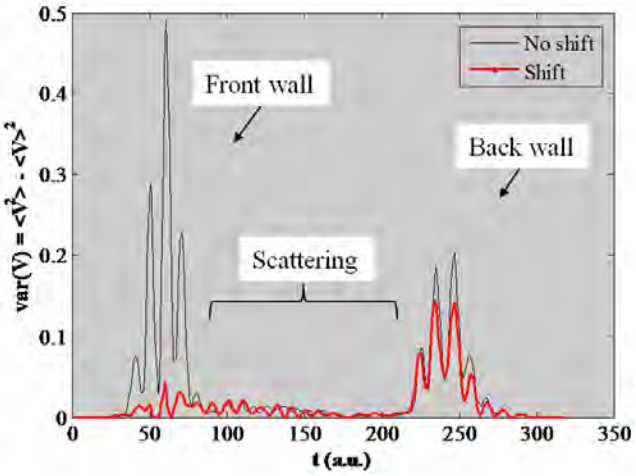

Figure 3.11: Resulting variances from Figure 3.10.

The variance has another interesting property. If the mean value is close to zero then the second term $< V >^2$ is approximately zero and therefore not very important for studying the scattering. This point is highlighted in Figure 3.12. For this result 2250 scan points were used. It is seen that the scattering between the front and back wall is close to each other.

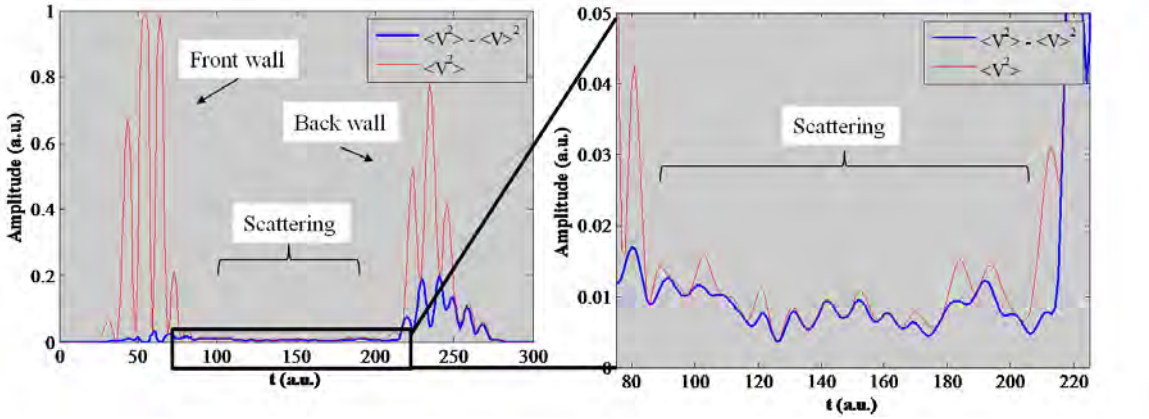

Figure 3.12: The second term's influence on the variance.

3.3.2 Parametric Analysis of the Number of Acquired Signals

Since there are variations in all materials such as surface, thickness and intrinsic variations, one has to find a suitable number of scan points M that gives a good profile of the material. Too few scan points can give a spatial variance that is largely affected by a local anomaly. On the other hand too many scan points over a large area can give a variance that is affected by fixtures and instruments that never can be perfectly aligned and in level.

Parametric analysis has been carried out on CFRP made of 1.2 mm thick T700 Toray fibers and an epoxy matrix. Two analyses were done with two different sample fixtures, as shown in Figure 3.13. The fixture to the left in the figure is called fixture A and the other one is called fixture B. In Table 3.4 one can see the differences between the set-ups. Both tests were done in perpendicular echo mode.

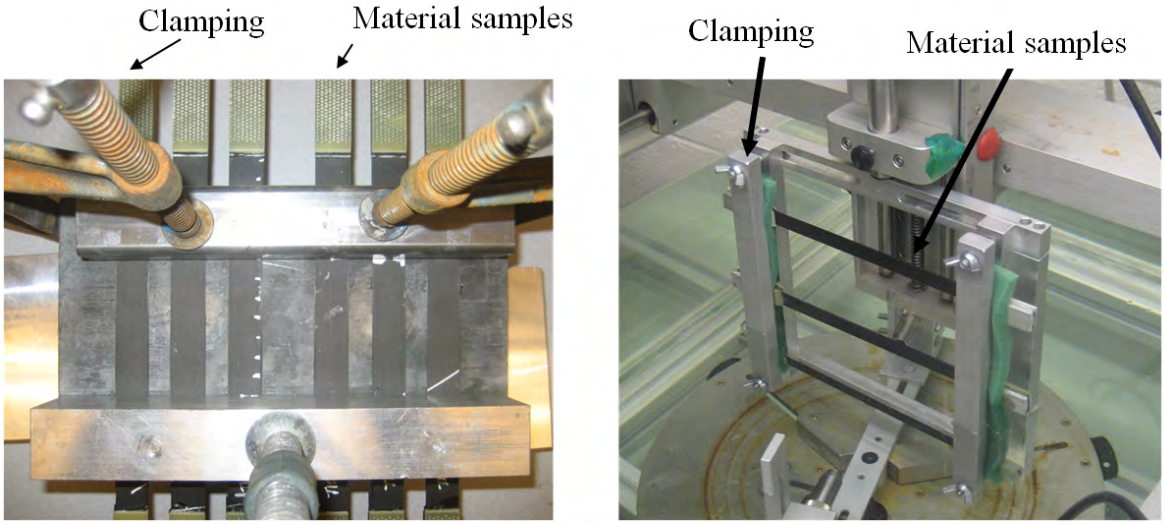

Figure 3.13: Left: Fixture A, Right: Fixture B.

Table 3.4: Experimental set-up and P/R settings for the parametric analysis of the number of acquired signals.

	Old fixture	**New fixture**
Experimental set-up	⊥ echo	⊥ echo
Transducer freq. (MHz)	15	25
Rel. Gain (dB)	35	55
Pulse Amp.	9	9
Pulse Energy	1 low z	1 low z
Damping	9	9
Free Backwall	No	Yes

The number of scan points used to calculate the variance is from 25 to 2400. In Figure 3.14 one can see how the variance changes with the increasing number of scan points. It is not obvious what number of scan points is the optimum, but it is clear that 25 and 50 scan points are diverging from all the other values and therefore 50 or less scan points are not sufficient. 100 and 200 scan points gives a similar result, and from 400 to 2400 scan points, the result starts to diverge from each other. Several hundred points are time consuming to collect and takes a lot of computer power to work with. Therefore 100 points were chosen for all upcoming experiments.

An interesting and important notice is that the result is consistent between the two fixtures.

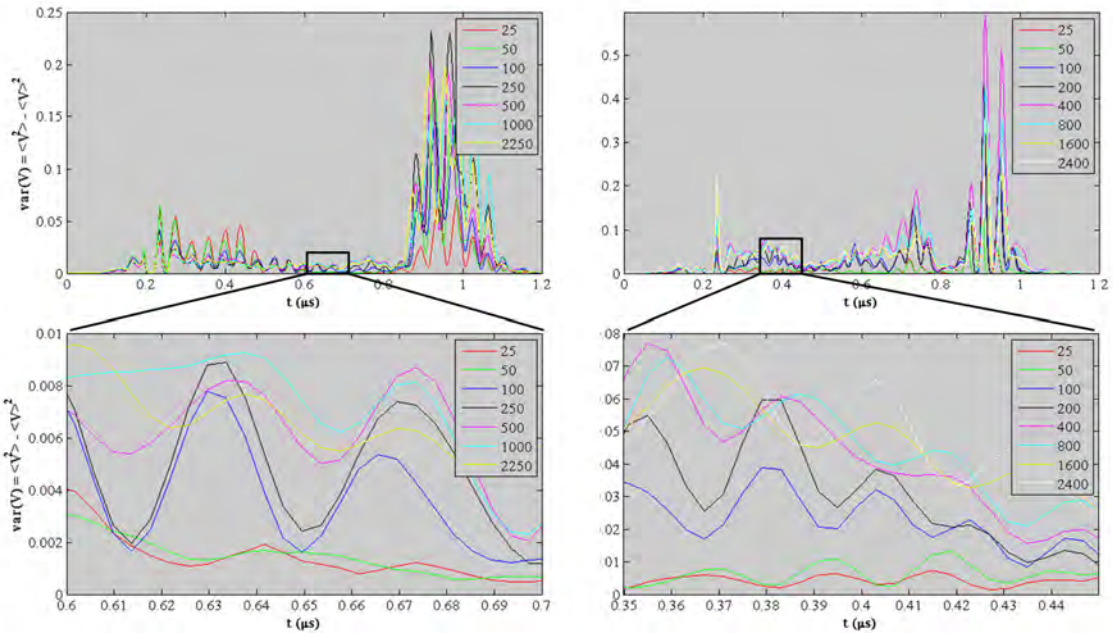

Figure 3.14: Left: Fixture A, Right: Fixture B.

3.3.3 Parametric Analysis of the Angle of Incidence

It is known that interlaminar cracks can act as kissing cracks which can be invisible for compressional waves [22, 23]. In the curing of advanced composites a temperature of 180 °C is common, and since the thermal expansion coefficient of carbon fibers is approximately zero the matrix will be in tension at room temperature. Furthermore it is then likely that also broken fibers can act as kissing cracks.

For the detection of interlaminar kissing cracks it has been shown that shear waves can be used, and that comes as a consequence from the fact that interlaminar cracks cannot transfer shear waves efficiently [22, 23]. Hence it seems reasonable that the same approach for fiber breakage could be effective. On this basis it was

decided that all experiments will be with inclined sonification. Parametric analysis of the angle of incidence was carried out to find critical angles for two types of experimental set-ups: in-line through transmission and polar through transmission. Schematics are found in Figure 3.15.

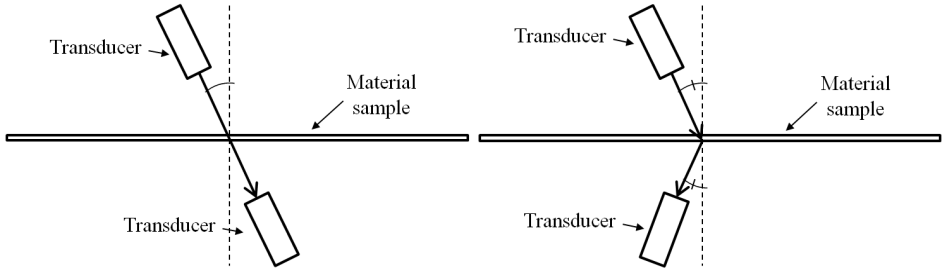

Figure 3.15: Left side: In-line through transmission, Right side: Polar through transmission.

In-line Through Transmission

In-line through transmission has been used to find the critical angles for the CFRP samples. Starting at 0° and using increments of 5° up to 35° gives a critical angel around 20 - 25°. Figure 3.16 shows the peak that was used to study how the amplitude changes with the the angle, and Figure 3.17 shows the relative amplitude $20log\frac{V}{V_0}$, where V_0 is for zero degrees angle of incidence. The amplitude is highest at 20 - 25°, which is believed to be where the second critical angle is found.

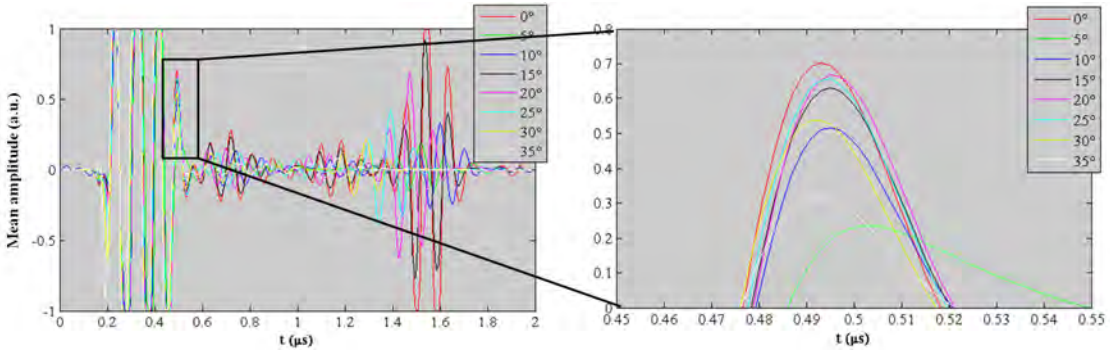

Figure 3.16: Ultrasonic signal in relation to angle of incidence.

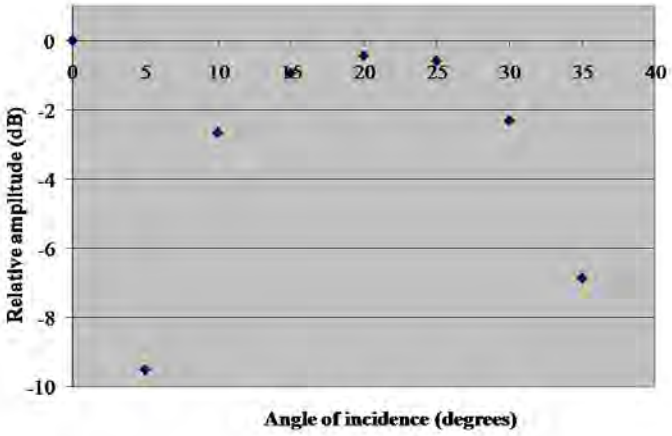

Figure 3.17: Amplitude relative to zero degrees of incidence.

The in-line through transmission was done with 25 MHz transducer. P/R settings are found in Table 3.5. No theoretical calculations were carried out due to transversely isotropic material which would make it difficult due to additional coupling effects besides Poission's effect etc.

Table 3.5: Experimental set-up and P/R settings for the in-line through transmission parametric analysis.

Experimental set-up	Inline through
Material used	CFRP
Transducer freq. (MHz)	25
Rel. Gain (dB)	55
Pulse Amp.	9
Pulse Energy	1 low z
Damping	9

Polar Through Transmission

A study of the angle of incidence was also done in a polar through transmission set-up, as shown in Figure 3.15. In such set-up only the scattering is seen and no front or back wall. According to the theory of acoustics diffuse scattering is the same in all directions and therefore the results should be the same in both polar through and polar echo set-up. The spatial variance experiments in the next chapter have been done in both polar modes but the parametric study was done in polar through transmission only.

Starting at 0° using increments of 2.5° up to 30° gives critical angles around 10° and 25° with the use of Gaussian curve fitting, $ae^{(-\frac{x-b}{c})^2}$, where a peak and a plateau can be seen at 10° and 25° (Figure 3.18). The two first values, 0°and 2.5°in Figure 3.18-19 gives faulty curve fittings since the front and back wall echo is separable and gives two regions of intense scattering instead of one.

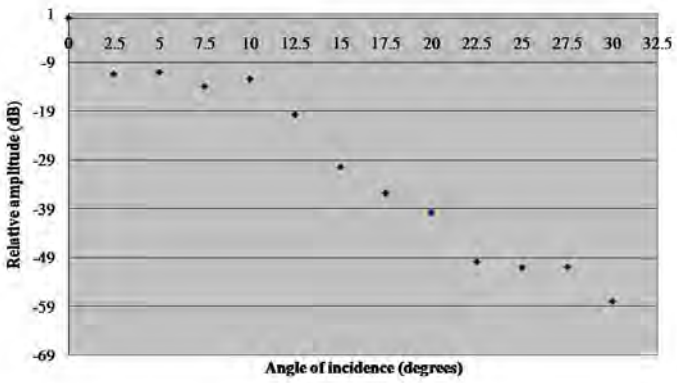

Figure 3.18: Maximum amplitudes from Gaussian curve fitting.

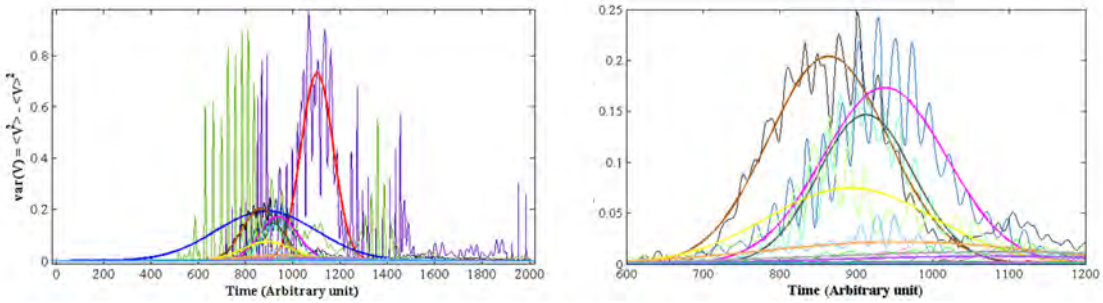

Figure 3.19: Left side: All variance curves from 0-30°, Right side: Without the faulty curve fittings, i.e. shows 5-30°.

The mean signal response and the variance for the critical angles 10° and 25° are plotted in Figures 3.20-21. From Figure 3.20, left hand side at 10° incidence one can see a large response around 100 μs, which comes from waves taking the shortest possible way between the transducers. At 25° this response is outside the time window (Figure 3.20, right hand side). The phenomen is illutrated in Figure 3.22. As seen in Figure 3.20, the response from the shortcut has very small variance. It was also seen during the experiment that the shortcut response did not change from scan point to scan point. The shortcut response dissapeared when a screwdriver was put in the immersion tank in the path of the shortpath. One explanation of why this shortcut responce has almost no varaince has been proposed. The ultrasonic wave

at such an oblique angle of the transducers axis is very weak and therefore the only ultrasonic energy reaching the receiving transducer has reflected from the sample next to the sample under test, or diffracted from the edge of the sample under test. In Appendix B one can see a figure of how close the GFRP samples were during the experiments.

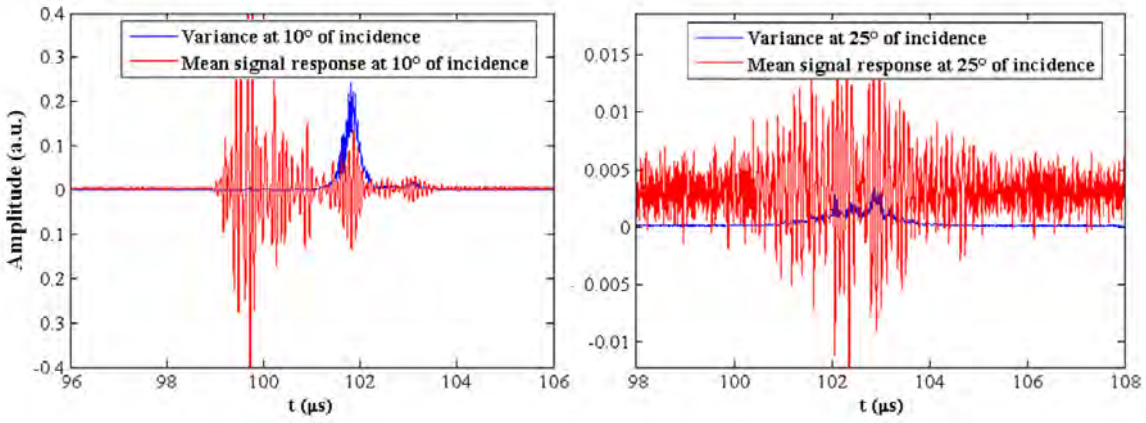

Figure 3.20: Mean signal response and variance at the; Left side: 1st critical angle, Right side: 2nd critical angle.

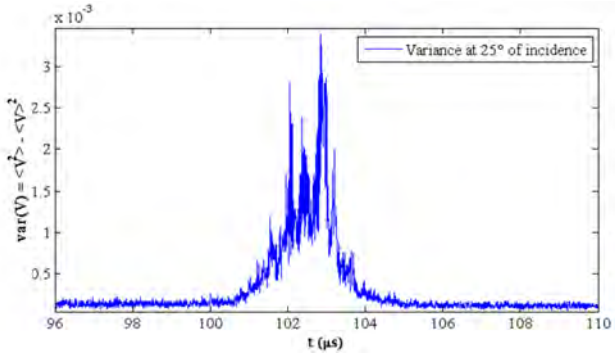

Figure 3.21: The variance at the 2nd critical angle, i.e. the same as Figure 3.20 right hand side.

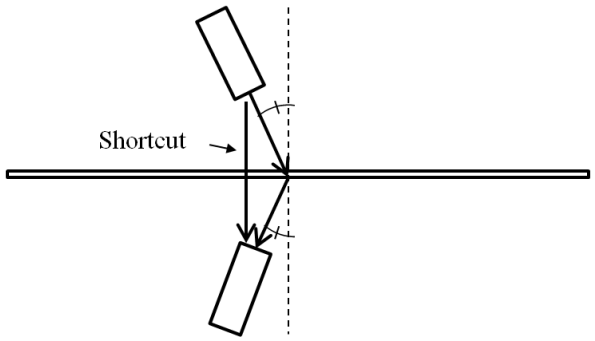

Figure 3.22: Illustraion of how the ultrasound wave takes a shortcut.

3.3.4 Experimental Procedure

Unidirectional CFRP and GFRP with a fiber diameter of 7.0 μm and 16.5 μm, respectively, were selected for the experiments. Five to six samples were used in each experiment for averaging. The experiments were done in the following way (Figure 3.23):

1. Ultrasonic testing of virgin samples.
2. Tensile loading to a certain percentage of ultimate tensile strength.
3. Repetition of the first two steps with increased loading.
4. Analysis of data.

Figure 3.23: The experimental procedure.

The ultrasonic testing was done with five different set-ups called A, B, C, D and E, as given in Figure 3.24. The angles of incidence used are 10 °and 25 °. The number of scan points was chosen as 100. All curves in experiment A were shifted for normalization.

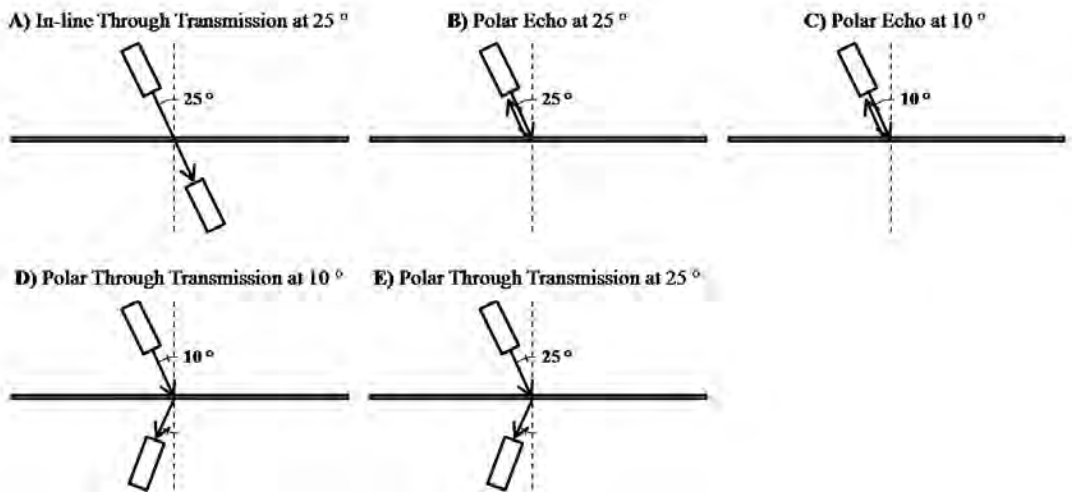

Figure 3.24: The five different experimental set-ups called A to E.

Chapter 4

Results: Diffuse Ultrasonic Testing of Advanced Composites

In this chapter the results from diffuse ultrasonic testing are presented. The tensile loading and ultrasonic testing cycle was accomplished, followed by variance calculation and analysis of the scattering.

Experiments were carried out on three sets of samples. Two sets were of the CFRP material and one set was of the GFRP material. The resolution was 200 μm over a 2x2 mm^2 area, giving 100 points. At each scan point an average of 90 signals was taken. P/R settings for the three sets of samples are given in Table 4.1.

Table 4.1: P/R Settings for the diffuse ultrasonic testing.

	CFRP - Set 1	**CFRP - Set 2**	**GFRP**
Transducer freq. (MHz)	25 s.f.	25 s.f.	25 s.f.
Rel. Gain (dB)	70	79	75 (55 for set-up A)
HP Filter (MHz)	7.5	7.5	7.5
LP Filter (MHz)	35	35	35
Pulse Amp.	9	16	16
Pulse Energy	1 low z	2 low z	2 low z
Damping	9	1	1

A measure of the amount of scattering within a material can be acquired by integrating the variance between the front and back wall. Shear waves have a lower wave speed than longitudinal waves and will therefore have a longer time of flight than longitudinal waves. The scattering can come from both longitudinal and shear waves and because of the different wave speeds the scattering signal arrives at different times. Therefore the scattering closer to the front wall seen by studying the variance is thought to be from longitudinal waves and the scattering closer to the back wall is thought to be primarily from shear wave interactions. Previous research shows that shear waves are more sensitive to interlaminar cracks [19, 20, 21, 22, 23]. The same should be true for fiber cracks due to the same orientation of the crack faces. On this basis the result of the integrated scattering can depend on what part of the scattering is studied.

Diffuse scattering is random scattering in random directions. With fiber breakage the number of scattering points increases and consequently the scattering should increase with fiber breakage. The expectation is therefore that the scattering goes up with fiber breakage.

In this thesis the scattering has been measured by integrating the variance over various time windows by using trapezoidal method in MATLAB. For each experimental set-up, one to two time widows have been arbitrarily selected depending on how the scattering looks and used for all samples through all damage states.

4.1 Carbon Fiber Reinforced Plastics

4.1.1 CFRP Samples - Set 1

In the first set of CFRP samples experimental set-up A was done, i.e. in-line through transmission at 25 °. Six samples were used. The experiment started with ultrasonic scanning of all six virgin samples. Thereafter loading of the samples was carried out before the next ultrasonic scanning. Loading levels were 0, 20, 40, 50, 60, 70, 80, 85 and 90 percent of ultimate tensile strength. In Figure 4.1 one can see all A-scan signals and variances from all damage states, i.e. 5400 signals (6 samples $\cdot$ 9 damage states $\cdot$ 100 signals = 5400) and 54 variance curves. In the same figure one can also see two time windows marked out, 0.75 - 1 μs and 1 - 1.2 μs. By integrating the variance in these time windows one receives a measurement of the scattering inside the material. In Figure 4.2 one can see the integrated values of all samples at their different damage states. The black squares are the mean value of the integrated scattering of the six samples at each damage state. The spread in the data is quite high and therefore no curve fitting have been applied due to a R^2 value that would be low. Instead visual inspections for trends are done. The left hand side shows the result from time window ”a” and right hand side shows the result from time

window ”b”. In both cases the trend is going down, contrary to the expectation.

Two time windows were chosen because if the received signal contains information from both shear and compressional wave they will arrive at different times due to the different wave speeds in the sample.

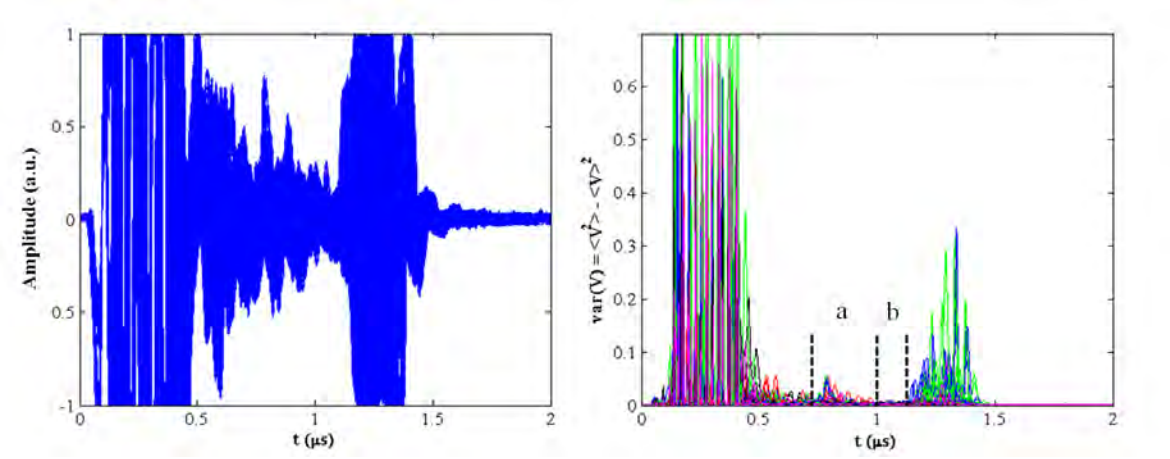

Figure 4.1: Left side: All signals from all damage states , Right side: All variances from all damage states. Time windows are marked out, ”a” and ”b”.

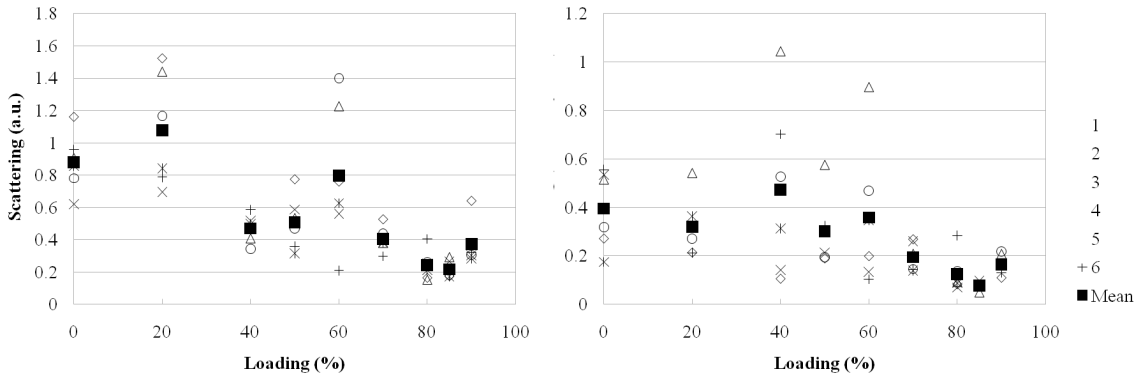

Figure 4.2: Integration of time windows; Left side: ”a” , Right side: ”b”.

4.1.2 CFRP Samples - Set 2

The same procedure as in the previous set was used for set 2, but for these samples all five different set-ups were examined. In these experiments five samples were used instead of six. Loading levels were 0, 20, 30, 40, 50, 60, 70, 80 and 85 percent of ultimate tensile strength.

It is not possible to make a direct comparison of set-up A for sample set 1 and 2 since the P/R settings are different. The gain, pulse amplitude, pulse energy and the damping are different. The only difference besides the P/R settings is in the shipment. The material for sample set 2 is from a later shipment from the supplier. By comparing Figure 4.1 and 4.3 one can see that the front and back wall are at the same position. By studying the scattering it is found to be much larger in sample set 2. The reason for this is not known. The trend is flat or going down with increased loading. Set-up B is at 25° polar echo and therefore only scattering is received, Figure 4.5. In Figure 4.6 one can see that the trend is down when the variances are integrated from 4 - 9 μs. Set-up C is at 10° polar echo. There appears to be some scattering from the front wall and some from the back wall, Figure 4.7. Tests have not been done to verify this. Three peaks can be seen in Figure 4.7 but the first peak has a very small variance. The time difference from the middle of the first peak to the middle of the third peak is two micro seconds. The time difference is the same in set-up D where the peak from the verified shortcut is found, Figures 4.9. Therefore it is belived that the first peak in Figure 4.7 is from the shortcut, but in polar echo mode instead of polar through transmission. Two time windows were picked where the trends are found to be down, Figure 4.8. Set-up D is at 10° polar

through transmission mode. This set-up is similar to set-up C. The amplitude of the variance is of the same order as in set-up C but two distinct peaks are not observed (Figure 4.9). All signals from through transmisson have information about both the front and the back wall, which can be an explaination for the difference. The variance shows a trend slightly upward for the first time window and slightly downward for the second time window, Figure 4.10. Set-up E is at 25° polar through transmission. Only the scattering is received like in set-up B. Integration of the scattering from 6.3 to 9 μs gives a trend going up, Figures 4.11-12.

Something that has to be known in set-up D and E is that the accuracy of the angle of incidence is unknown. In the later experiments on the GFRP samples it was found out that the protractor was not moving together with the fixture as it was meant to do, see Appendix B. Therefore the angle of incidence can differ by some degrees from 10° and 25° in set-up D and E.

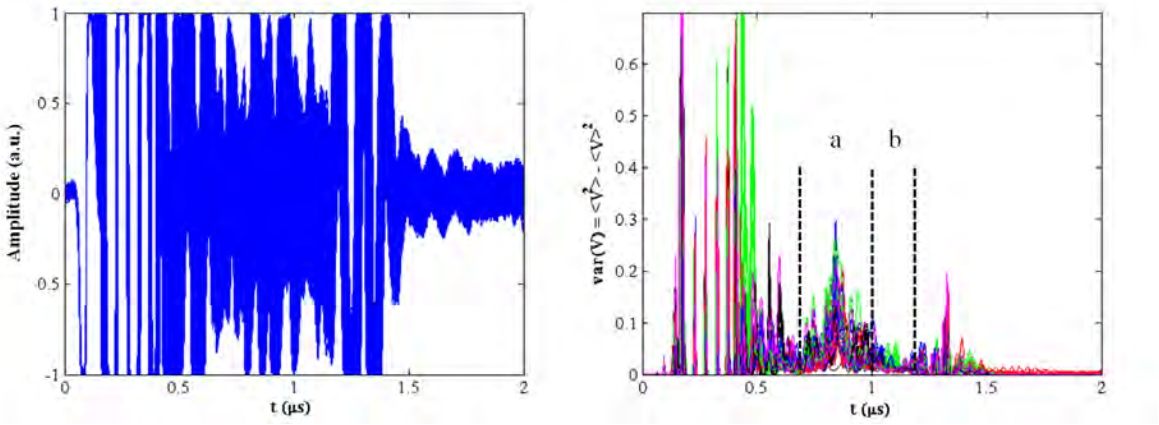

Figure 4.3: Set-up A: All signals from all damage states and the corresponding variances. Time windows marked out ″a″ and ″b″.

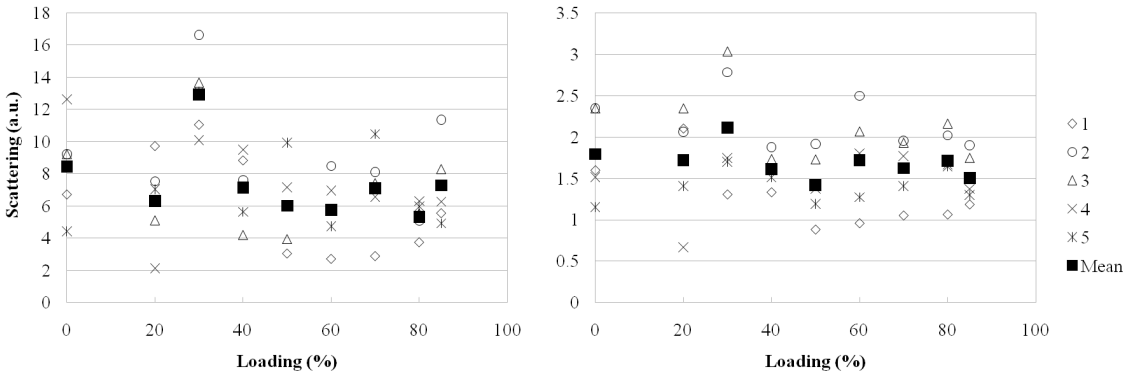

Figure 4.4: Set-up A: Integration of time windows ″a″ and ″b″

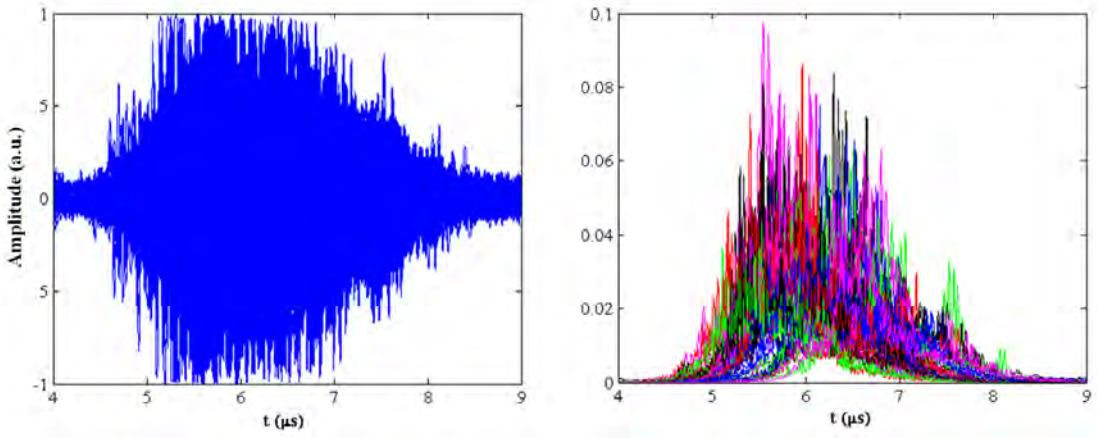

Figure 4.5: Set-up B: All signals from all damage states and the corresponding variances.

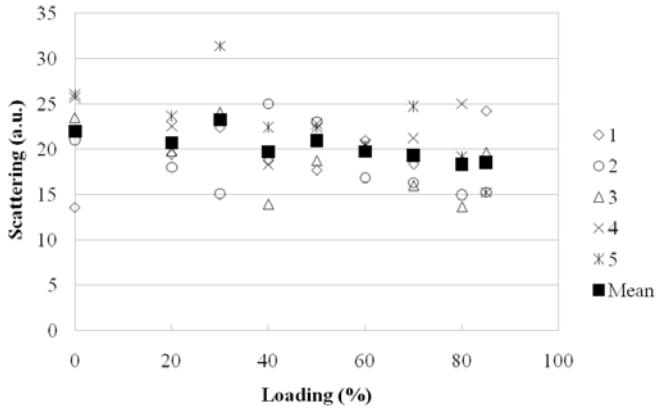

Figure 4.6: Set-up B: Integration of time window, 4 - 9 μs.

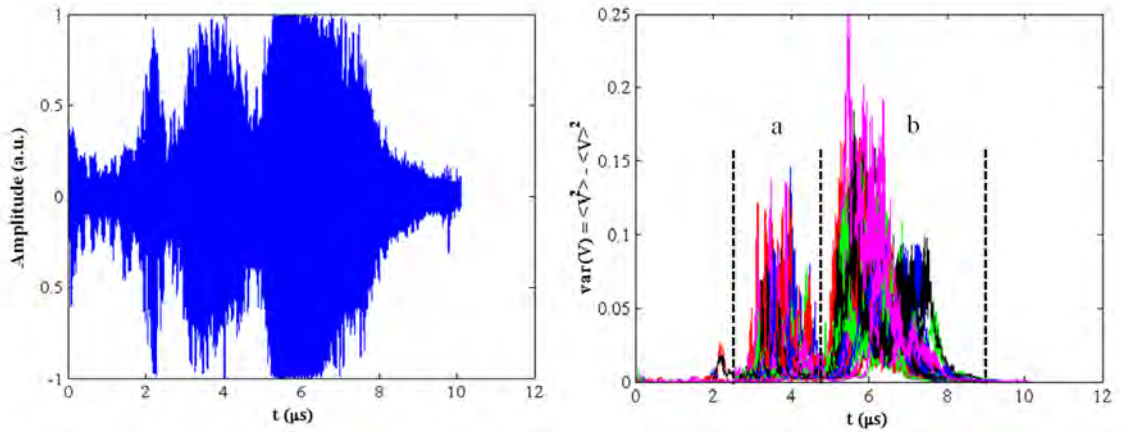

Figure 4.7: Set-up C: All signals from all damage states and the corresponding variances. Time windows marked out ″a″ and ″b″.

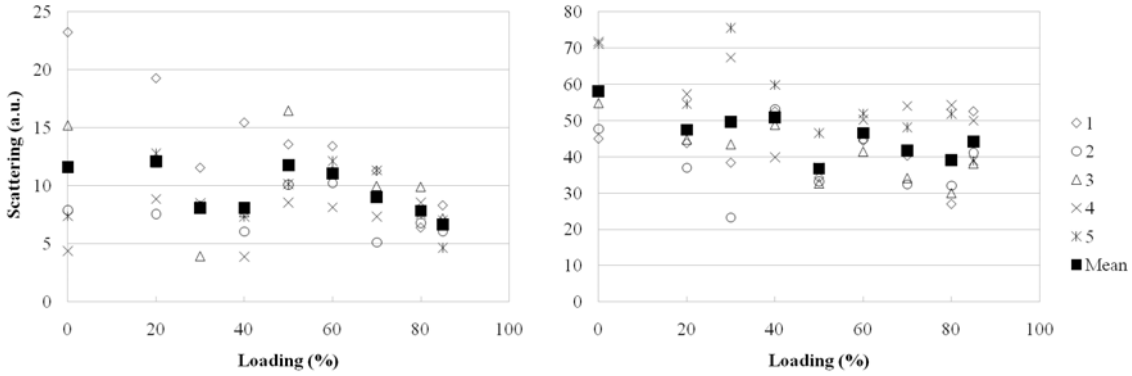

Figure 4.8: Set-up C: Integration of time windows; Left side: ″a″ , Right side: ″b″.

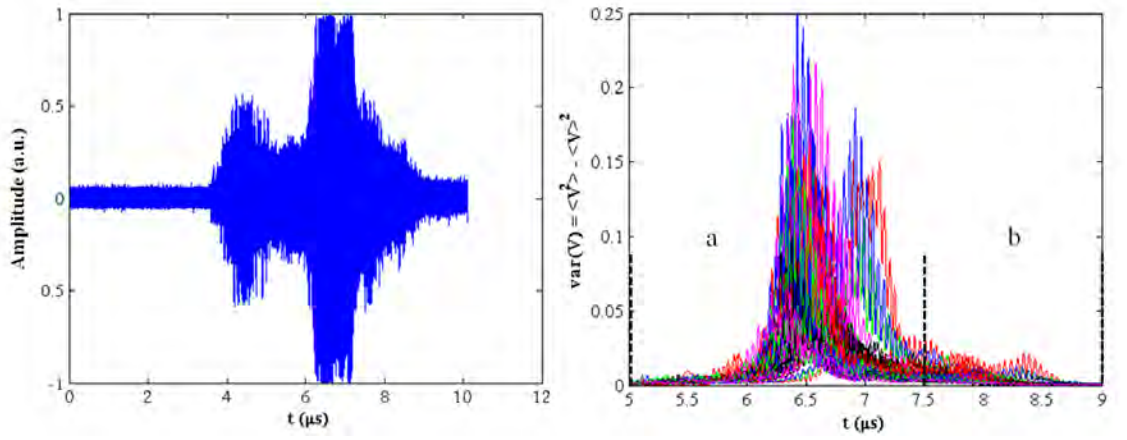

Figure 4.9: Set-up D: All signals from all damage states and the corresponding variances. Time windows marked out ″a″ and ″b″.

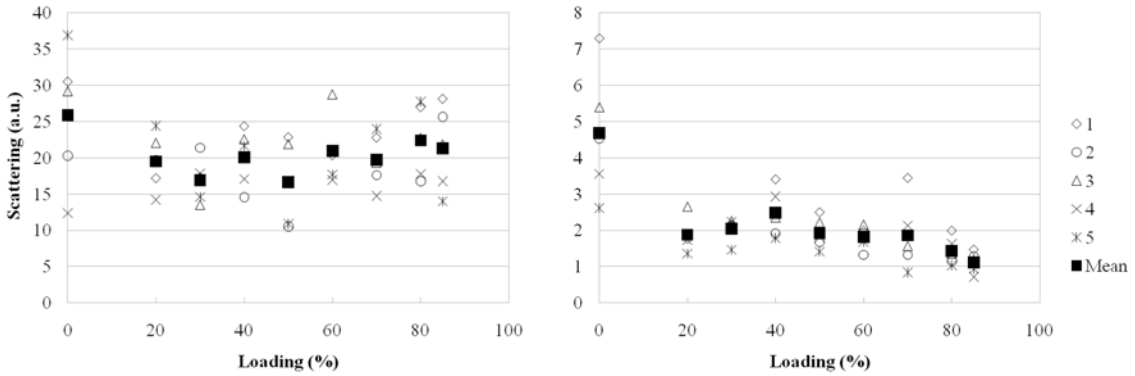

Figure 4.10: Set-up D: Integration of time windows; Left side: ”a” , Right side: ”b”.

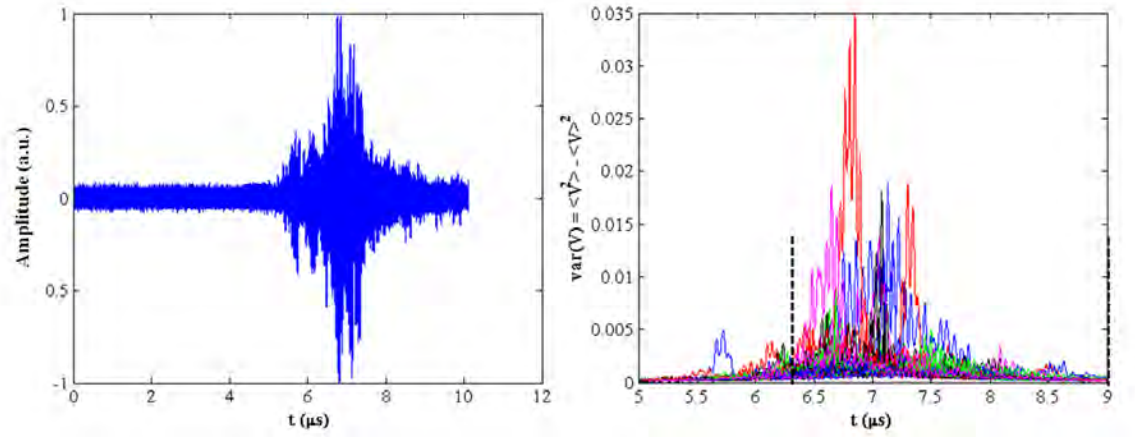

Figure 4.11: Set-up E: All signals from all damage states and the corresponding variances. Time windows marked out from 6.3 - 9 µs.

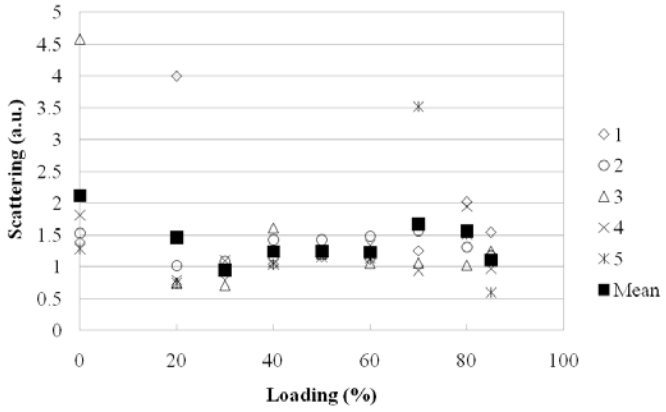

Figure 4.12: Set-up E: Integration of time window, 6.3 - 9 µs.

4.2 Glass Fiber Reinforced Plastics

Five samples of GFRP were examined in the same way as the CFRP for comparison of composites with different fiber diameter. Loading levels were 0, 50, 60, 70, 80 and 90 percent of ultimate tensile strength.

Set-up A is at 25° in-line through transmission. At a frequency of 25 MHz the attenuation in the material is to high to be able to see the back wall clearly, but the time of flight between the front and the back wall is known to be 0.8 μs (Figure 3.5). An integration can therefore be done without integrating the back wall. The variance trend is flat or down, Figures 4.13-14. Set-up B is at 25° polar echo and therefore only scattering is received, Figure 4.15. The first integrated variances at zero percent loading are diverging from the rest by an unknown reason. The variance trend is up, see Figures 4.15-16. Set-up C is at 10° polar echo. The resulting variance is similar to the one received for CFRP samples in set-up C, but the GFRP samples are thinner so the peaks are closer to each other. As in the previous set-up, the integrated scattering of the virgin samples diverges. The variance trend is flat or down (see Figures 4.19-20). In Figure 4.17, set-up C, and Figure 4.19, set-up D, there is some scattering between 0 - 4 μs that has a very small variance. This is similar as for the CFRP samples where the signal is taking a shortcut. In the polar through transmission set-up D the scattering trend is going down with loading, see Figures 4.19-20. And for the last set-up E the trend is flat or going up, Figures 4.21-22.

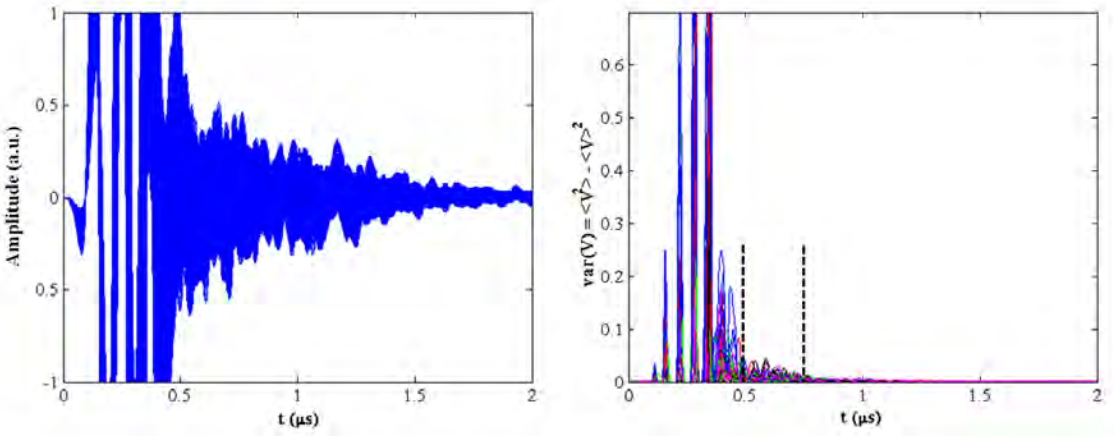

Figure 4.13: Set-up A: All signals from all damage states and the corresponding variances.

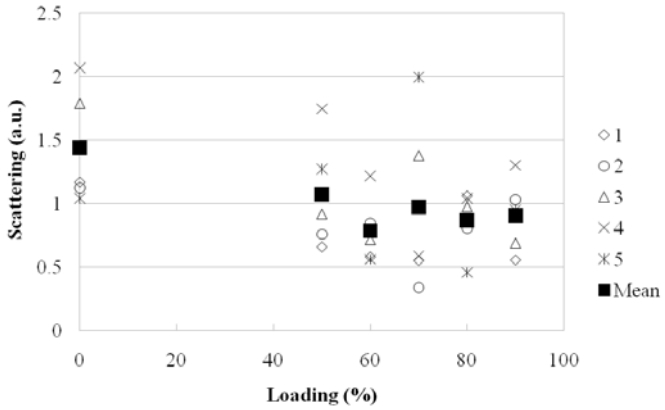

Figure 4.14: Set-up A: Integration of time window, 0.5 - 0.75 μs.

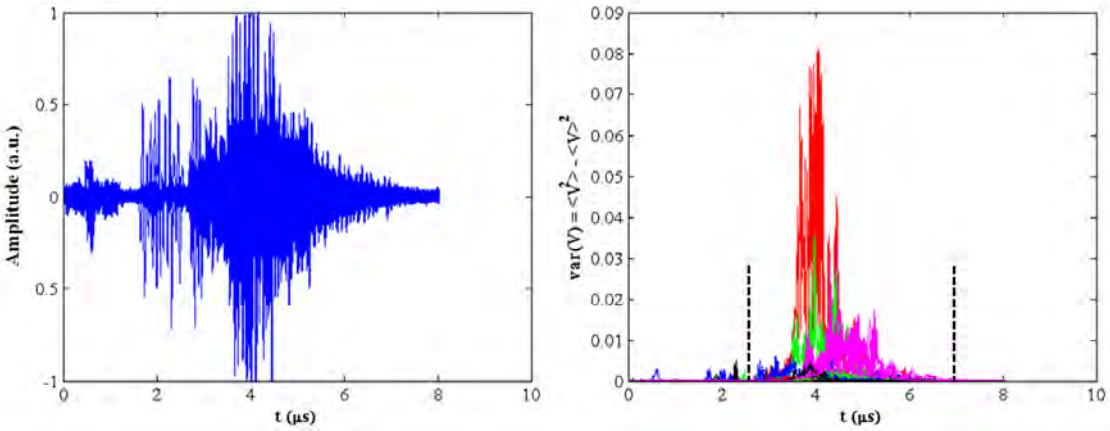

Figure 4.15: Set-up B: All signals from all damage states and the corresponding variances.

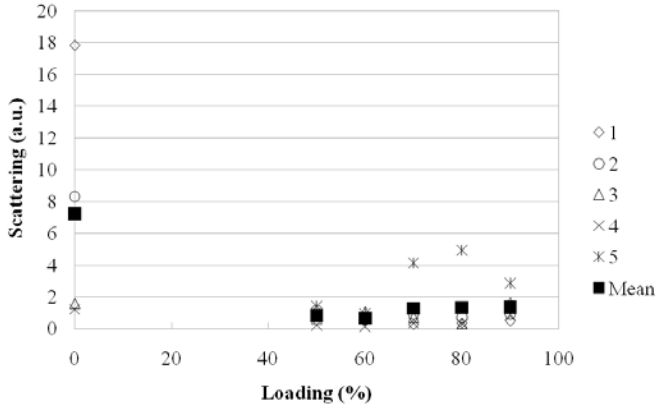

Figure 4.16: Set-up B: Integration of time window, 2.6 - 7.0 μs.

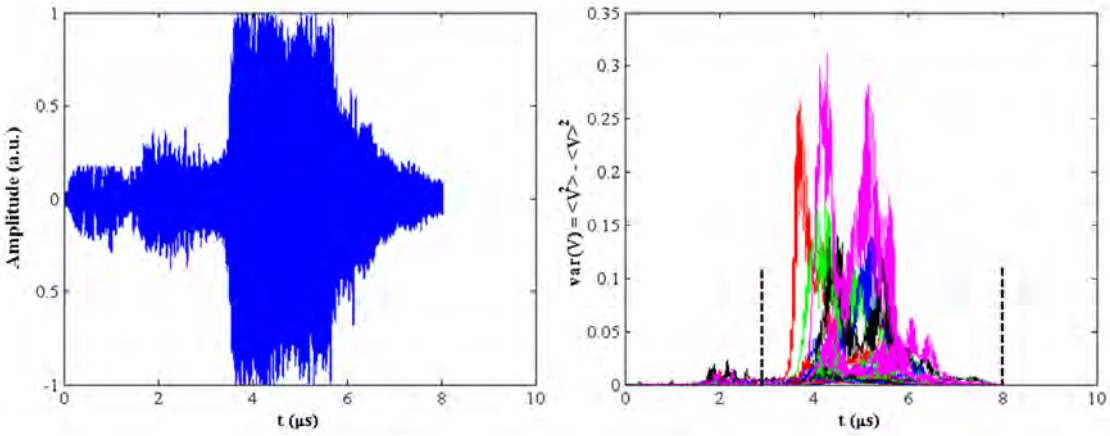

Figure 4.17: Set-up C: All signals from all damage states and the corresponding variances.

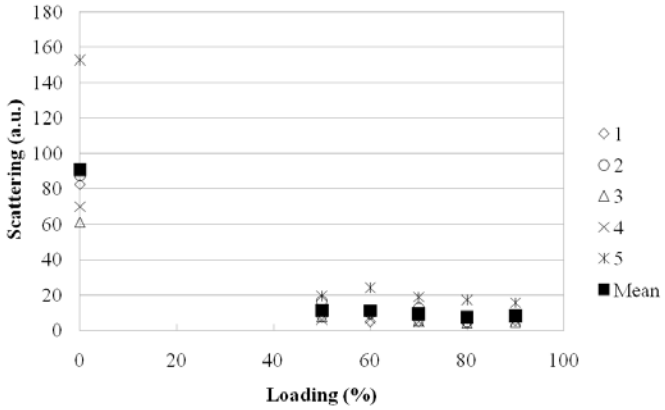

Figure 4.18: Set-up C: Integration of time windows, 3.0 - 8.0 μs.

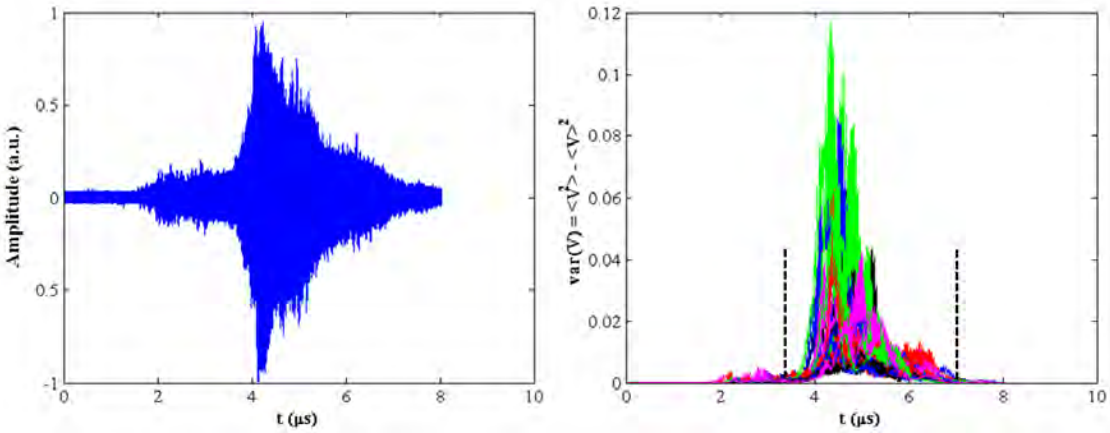

Figure 4.19: Set-up D: All signals from all damage states and the corresponding variances.

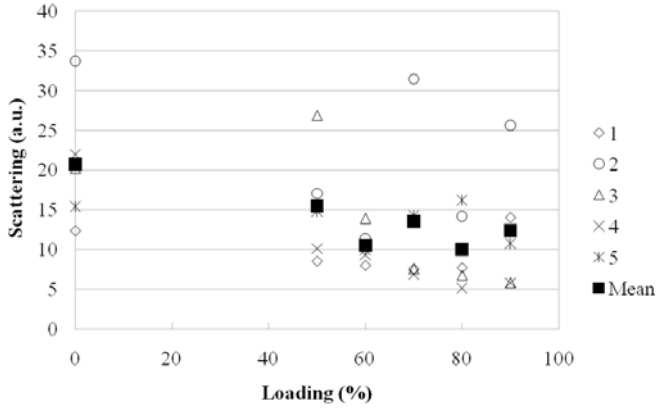

Figure 4.20: Set-up D: Integration of time window, 3.5 - 7.0 μs.

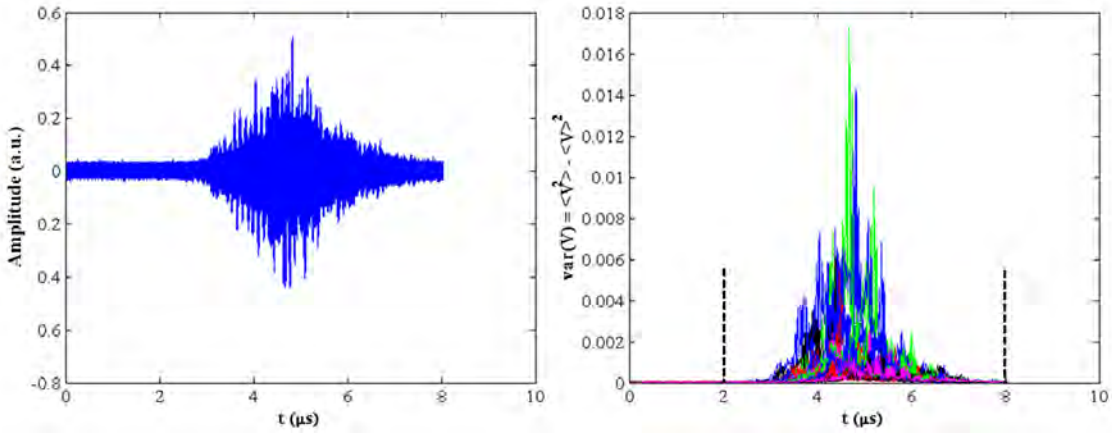

Figure 4.21: Set-up E: All signals from all damage states and the corresponding variances.

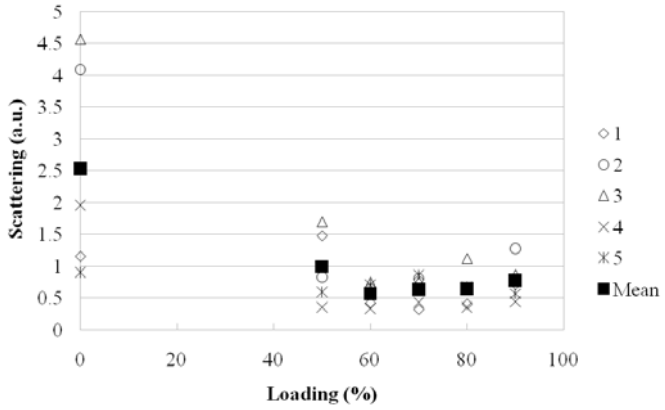

Figure 4.22: Set-up E: Integration of time window, 2.0 - 8.0 μs.

Chapter 5

Discussion and Conclusion

A consistent trend of the scattering with increased loading is not possible to distinguish in the result presented. The spread is large between the samples and therefore the statistical uncertainty is high. Due to this it was decided not to do any curve fittings because the R^2 value would be low. Instead a visual examination of how the scattering changed with increased loading was done. In most cases the the scattering is decreasing with increased loading, thus increased fiber breakage. This contradicts the assumption of increased scattering with more fiber breakage. It can be missleading results or a lack of the understanding of the physics behind this phenomena.

The variance was integrated between the front and the back wall to give a measure of the scattering within the materials. One or two time windows was chosen depending on the set-up and how the scattering appeared. This was done because of the different time of flight of longitudinal and shear waves due to their unique wave speeds and for their respective sensitivity to crack faces in the fiber direction.

By looking at the results above, one cannot see any difference in the trends between the first time window and the later ones.

In one case a more clear uptrend was observed. If the scattering in set-up A of CFRP sample set 2 is studied before the two time windows marked out in Figure 4.3, an upward trend is received, see Figures 5.1-2 below. But the opposite trend is found if the same time window and set-up is studied in the first CFRP set, see Figures 5.3-4. These two results shows that the reproducability is low, or the spread in data is too large. But there is also a possibility of difference in the second batch of material delivered from the supplier.

It is also seen that the scattering within the material in Figure 5.1 and 5.3 is very different. If this can be explained by the change in P/R setting (Table 4.1) cannot be answered.

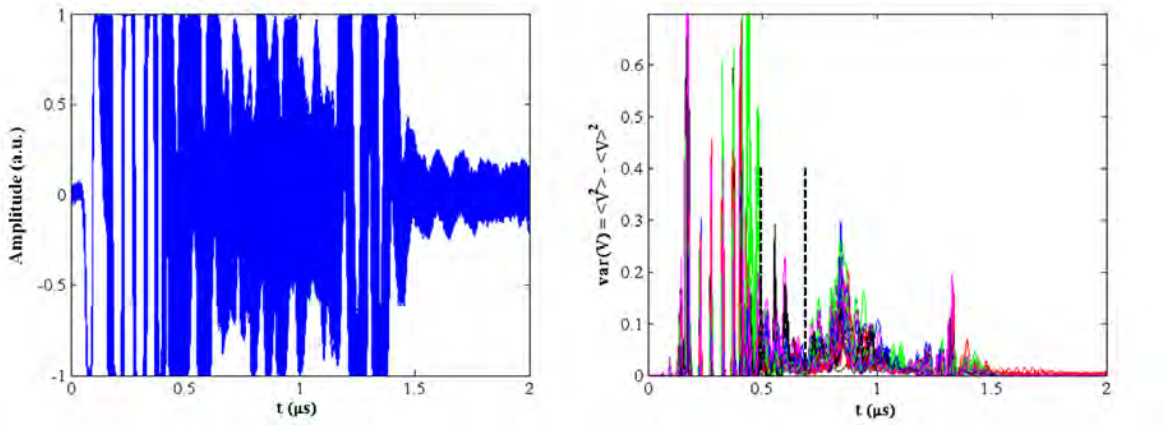

Figure 5.1: CFRP sample set 2, Set-up A: Left side: All signals from all damage states , Right side: All variances from all damage states. Time window is marked.

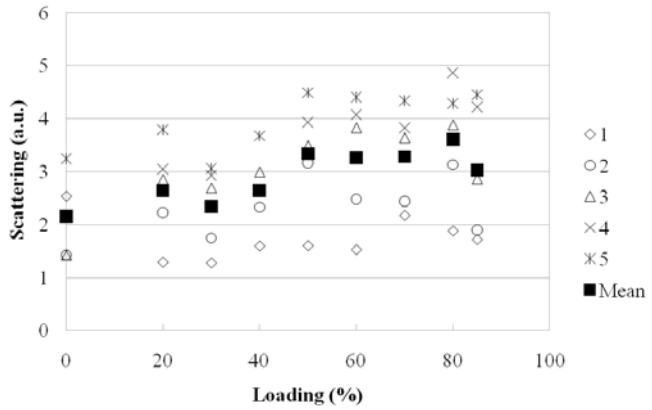

Figure 5.2: CFRP sample set 2, Set-up A: Integration of time window, 0.5 - 0.75 µs.

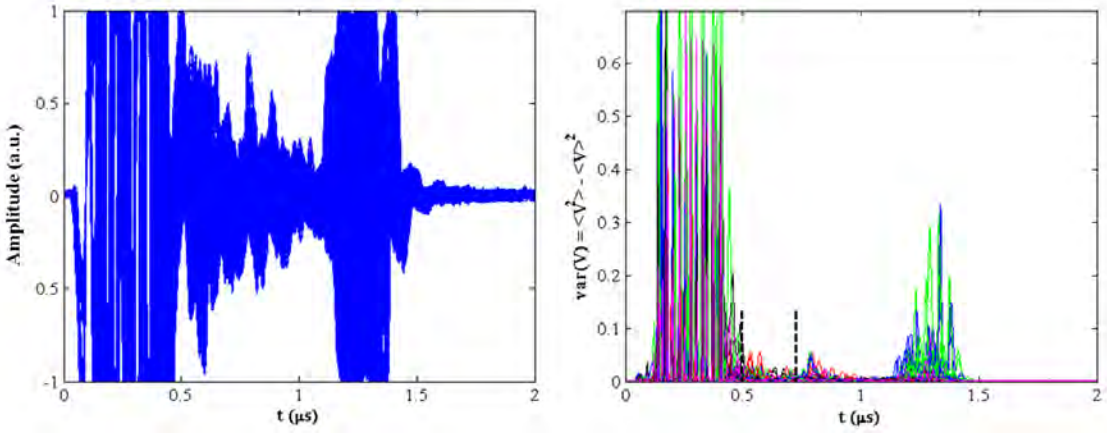

Figure 5.3: CFRP sample set 1, Set-up A: Left side: All signals from all damage states , Right side: All variances from all damage states. Time window is marked.

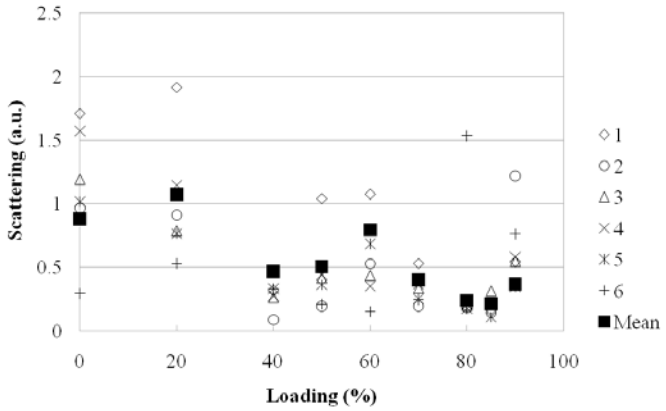

Figure 5.4: CFRP sample set 1, Set-up A: Integration of time window, 0.5 - 0.75 µs.

Some of the scattering of the virgin GFRP samples deviates from the loaded samples. This is seen in set-up B, C and E. These set-ups are 10° and 25° polar echo and 25° polar through transmission. For the undamaged samples the integrated scattering is higher than for all the loaded states, Figures 4.16, 4.18 and 4.22. The reason for this is unknown but with better fixtures the experimental set-ups can be easier to carry out with less risk for mistakes.

All experiments were performed with 100 acquired signals over an area of 2x2 mm with the resolution of 200 μm. The large spread in data can come from too few scan points or lack of precision in the set-ups. According to Figure 3.14, 25 - 50 signals seems to be too few but if for example 100 or 1000 signals are the optimal is hard to decide. How the set-up was done and calibrated can be seen in Appendix B. With improved fixtures with better precision the spread in data can be lowered.

According to Weibull distribution and acoustic emission it should be fiber breakage all over the samples when the load is approaching the ultimate tensile strength. And according to stress transfer between matrix and fibers, one fiber can have multiple breakage. Lack of fiber breakage is most likely not an issue.

Another explanation why the change in scattering cannot be seen is masking from the fibers. The acoustic impedance between the matrix and fibers is large and due to that there is multiple scattering at the microscale. This scattering is different due to the orientation of the interfaces of fiber and fiber breaks but at the same time this scattering must be much larger than the scattering from the fiber breakage. A theoretical model would be interesting for studying the scattering. Finite element modeling can be a promising method but it would demand a large amount of com-

puter power. Experiments showed that critical angles were found to be around 10 and 25 degrees from perpendicular incidence. In conclusion, it is clear that more research needs to be done in order to understand diffuse scattering in advanced composites.

In addition, two points of future research have been identified:

- Minimize spread and uncertainty in data by more extensive parameteric analysis of the number of scan points and with the use of improved fixtures.
- Develop theoretical model of the scattering for better understanding and comparison with experimental results.

Bibliography

[1] G. Marsh: *Finding Flaws in Composites*, Reinforced Plastics, vol. 46 (2002) p. 42-46.

[2] R.A. Smith: *Advanced NDT of Composites in the United Kingdom*, Materials Evaluation, Vol. 65 (7), (2007), p. 697-710.

[3] G. Ghoshal: *Diffuse Ultrasonic Scattering in Heterogeneous Media*, PhD Dissertation, Lincoln, NE, (2008).

[4] H. Kaczmarek: *Ultrasonic Detection of Damage in CFRPs*, Journal of Composite Materials, Vol. 29, (1995).

[5] A.E. Scott, M. Clinch, W. Hepples, N. Kalantzis, I. Sinclair, S.M. Spearing: *Advanced Micro-Mechanical Analysis of Highly Loaded Hybrid Composite Structures*, University of Southampton, SO17 1BJ UK.

[6] X.E. Gros: *Current and Future Trends in Non-destructive Testing of Composite Materials*, Annales de Chimie Science des Materiaux, 25, (2000), p. 539-544.

[7] D.K. Hsu: *Nondestructive Inspection of Composite Structures: Methods and Practice*, 17th World Conference on Nondestructive Testing, (2008).

[8] M.L. Costa, S.F.M. de Almeida, M.C. Rezende: *The Influence on Porosity on the Interlaminar Shear Strength of Carbon/Epoxy and Carbon/Bismaleimide Fabric Laminates*, Composites Science and Technology, 61 (14), (2001), p. 2101-2108.

[9] J.E. Zimmer, J.R. Cost: *Determination of the Elastic Constants of a Unidirectional Fiber Composite Using Ultrasonic Velocity Measurements*, Journal of the Acoustical Society of America, (1970).

[10] R.E. Smith: *Ultrasonic Elastic Constants of Carbon Fibers and Their Composites*, Journal of Applied Physics, Vol. 43, (1972).

[11] S.J. Wilkinson, W.N. Reynolds: *The Propagation of Ultrasonic Waves in Carbon-Fibre-Reinforced Plastics*, Journal of Applied Physics, Vol. 7, (1974).

[12] R.A. Kline: *Wave Propagation in Fiber Reinforced Composites for Oblique Incidence*, Journal of Composite Materials, Vol. 22, (1988).

[13] S.-C. Wooh, I.M. Daniel: *Mechanical Characterization of an Unidirectional Composite by Ultrasonic Methods*, Journal of the Acoustical Society of America, (1991).

[14] D.E.W. Stone, B. Clarke: *Ultrasonic Attenuation as a Measure of Void Content in Carbon-Fibre Reinforced Plastics*, Non-destructive Testing, Vol. 8 (3), (1975), p. 137-145.

[15] D.T. Hayford, E.G. Henneke, W.W. Stinchcomb: *The Correlation of Ultrasonic Attenuation and Shear Strength in Graphite-Polyimide Composites*, Journal of Compsoite Materials, Vol. 11, (1977).

[16] R. Prakash: *Non-destructive Testing of Composites*, Composites, (1980).

[17] D.J. Hagenmaier, R.H. Fassbender: *Ultrasonic Inspection of Carbon-Epoxy Composites*, Materials Evaluation, Vol. 43, (1985).

[18] Y. Bar-Cohen: *NDE of Fiber-reinforced Composite Materials - A Review*, Materials Evaluation, (1986).

[19] M.R. Gorman: *Ultrasonic Backscatter Imaging of Transverse Matrix Cracks*, Journal of Composites, Vol. 25, (1991).

[20] V.K. Kinra, A.S. Ganpatye, K. Maslov: *Ultrasonic Ply-by-Ply Detection of Matrix Cracks in Laminated Composites*, Journal of Nondestructive Evaluation, Vol. 25, (2006).

[21] K. Maslov, R.Y. Kim, V.K. Kinra, N.J. Pagano: *A New Technique for the Ultrasonic Detection of Internal Transverse Cracks in Carbon-fibre/Bismaleimide Composite Laminates*, Composite Science and Technology, Vol. 60, (2000), p. 2185-2190.

[22] J.-H. Shih, A.K. Mal, M. Vemuri: *Plate Wave Characterization of Stiffness Degradation in Composites During Fatigue*, Res. Nondestr. Eva., Vol. 10, (1998), p. 147-162.

[23] T. Kundu, A. Maji, T. Ghosh, K. Maslov: *Detection of Kissing Bonds by Lamb Waves*, Ultrasonics, Vol. 35 (8), (1998), p. 573-580.

[24] J.A. Turner: *Diffuse Ultrasonics for Inspection of Concrete*, Proceedings of SPIE - The International Society for Optical Engineering 4337, pp. 95-104 , (2001).

[25] G. Ghoshal, J.A. Turner: *Numerical Model of Longitudinal Wave Scattering in Polycrystals* , IEEE Transactions on Ultrasonics, Ferroelectrics, and Frequency Control 56 (7), art. no. 5116867, pp. 1419-1428 , (2009).

[26] G. Ghoshal, J.A. Turner: *Diffuse Ultrasonic Backscatter in a Two-dimensional Domain* , Acta Mechanica 205 (1-4), pp. 35-49, (2009).

[27] C.F. Buynak, T.J. Moran, S. Donaldson: *Characterization of Impact Damage in Composites*, SAMPE Journal 24 (2), pp. 35-39 , (1988).

Appendix A

Conventional Ultrasonic Testing of Advanced Composites

To be able to understand diffuse ultrasonic methods one has to understand conventional ultrasonic methods. In section A.1 the transverse wave speed of carbon fiber reinforced plastics (CFRP) is extracted. Section A.2 is dedicated to study the limits of conventional ultrasonics in the sense of detecting thin films of Teflon within CFRP.

A.1 Compressional Wave Speed in CFRP

Wave speeds have been measured for a block of aluminum and a block of unidirectional CFRP. The aluminum reference wave speed was taken from the NDT Resource Center and compared to the measured. The carbon fiber type in the CFRP block is unknown but it is not considered as a restriction. The objective is to make a rough estimation of the wave speed in the transverse fiber direction of CFRP so it can be

used later to identify and verify back walls. The fiber volume fraction in the CFRP block is estimated to be 0.6.

The thickness of the aluminum block was 76.35 mm and the length and thickness of the CFRP block was 95 mm and 17.9 mm respectively. In Table A.1 and A.2 one can see the set-up used and the calculated wave speeds from experiments. In Figure A.1 the wave speed was calculated at the points where the amplitude reach 0.4. In Figure A.2 the same was carried out for an amplitude of 0.2. In Figure A.3 the calculation was done at the minima indicated by the arrows.

Table A.1: P/R Settings for the wave speed experiments.

	Al	**CFRP - L**	**CFRP - T**
Method	Immersion	Hand held	Hand held
Transducer freq. (MHz)	15 s.f.	5 Unfocused	5 Unfocused
Rel. Gain (dB)	55	35	35
HP Filter (MHz)	12.5	2.5	2.5
LP Filter (MHz)	22.5	5	5
Pulse Amp.	16	16	16
Pulse Energy	4 low z	4 low z	4 low z
Damping	9	9	9

Table A.2: Measured compressional wave speed.

Material	**Wave Speed (m/s)**
Al	6340
Al Reference (NDT Res.)	6320
CFRP L	9260
CFRP T	3110

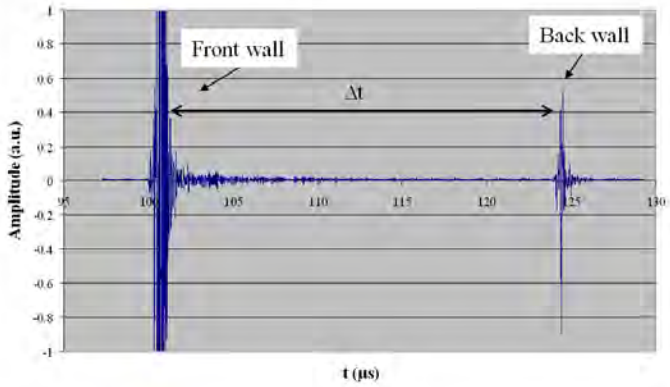

Figure A.1: A-scan of the aluminum block showing front and back wall.

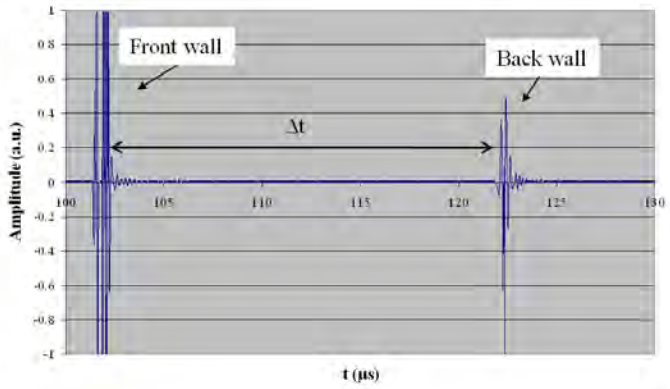

Figure A.2: A-scan from the longitudinal direction of the CFRP block showing front and back wall.

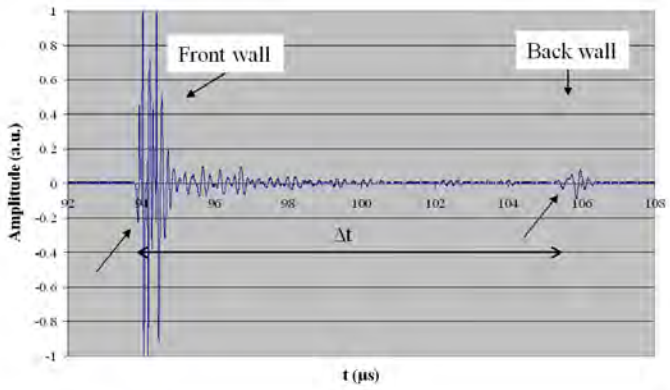

Figure A.3: A-scan from the transverse direction of the CFRP block showing front and back wall.

A.2 On the Limits of Conventional Ultrasonic Testing

Tests close to the limit of conventional ultrasonic for identification of delamination and Teflon foil has been done in a through-transmission set-up together with a 25 MHz focused transducer. The sample was made of eight 0-degrees Hexcel F3900 pre-pregs, 1.5 mm thick, with woven glass fiber on both sides, i.e. GF/CF/GF. In the middle of the pre-pregs it was partly a Teflon foil with an measured thickness of 115 μm was placed as a simulated delamination. If the compressional wave speed is between $3000 - 3500\ m/s$, a frequency of 25 MHz would then give a wave length of $120 - 140\ \mu m$.

In Figure A.4 one can see dots that are believed to be local high scattering points. In the left lower corner of the sample there is a delamination. From that corner the Teflon foil goes $45\,mm$ into the sample, from the left to the right. With the proper gate setting one can identify the area where the Teflon foil is located, see Figure A.5. The Teflon foil is easier to see in the A-scans in Figure A.6. The distance to the middle of the sample is $2.25\ mm$. With the use of Figure A.7 the wave speed can be calculated between the first arrow to the middle of the two arrows on the right hand side. The middle is chosen since the thickness of the Teflon foil is only 115 μm. By doing so one ends up with a compressional wave speed of $3250\ m/s$.

For the construction of the C-scans a resolution of 0.5 mm and an average of five A-scans were used for each point in the C-scan. With a higher resolution the edge of the Teflon foil would be sharper. In Figure A.8 one can see a C-scan from delaminated GFRP as a comparison. The set-up was in echo mode with a resolution of 200 μm. A 15 MHz transducer was used. As one can see it is not a straight edge

where the delamination ends.

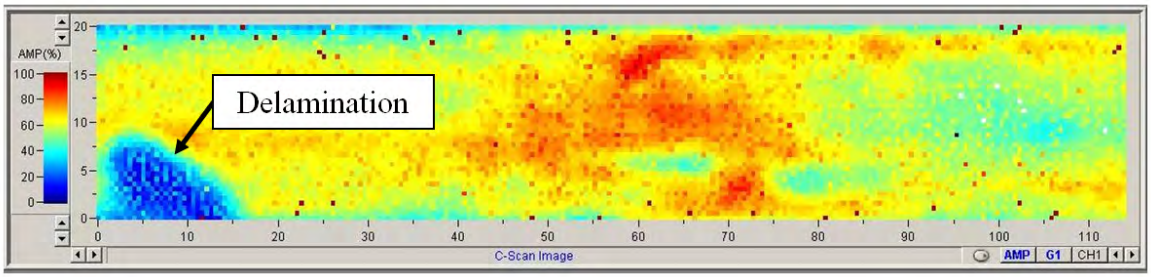

Figure A.4: 25 MHz through-transmission.

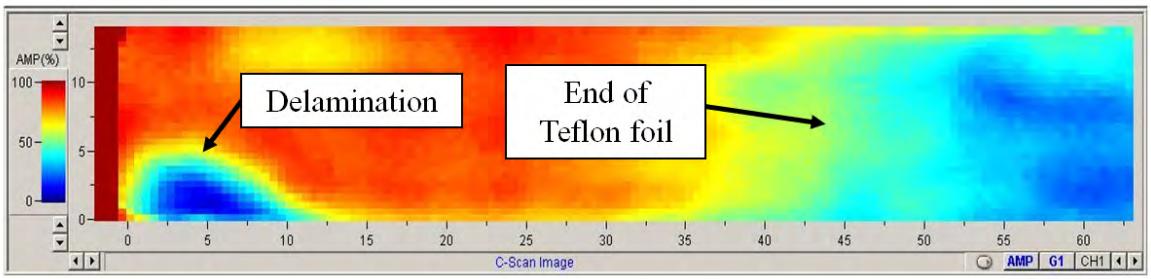

Figure A.5: 25 MHz through-transmission with the gate setting adjusted for identification of Teflon foil.

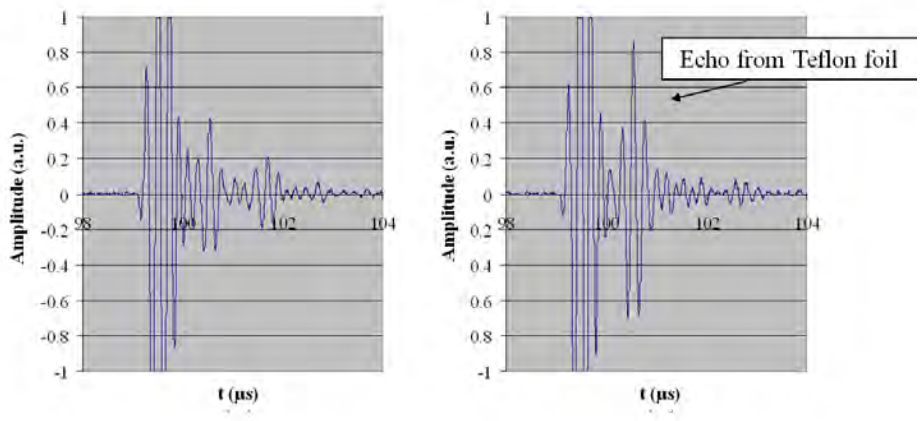

Figure A.6: 25 MHz through-transmission A-scan. Without and with Teflon foil.

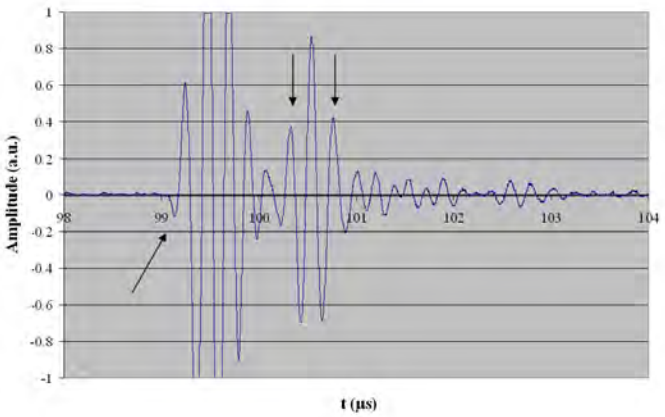

Figure A.7: Wave speed is calculated between the first arrow to the middle of the two arrows on the right hand side.

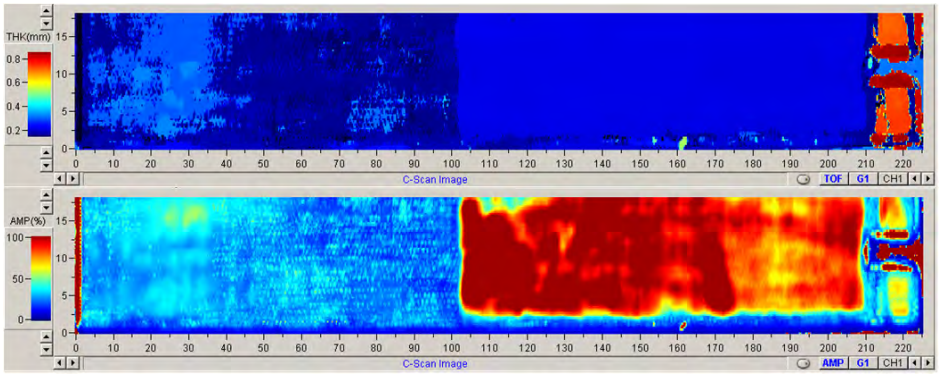

Figure A.8: Delaminated GFRP. 15 MHz transducer and a resolution of 200 µm.

Appendix B

Details of Experimental Equipment

In this appendix one finds a collection of photographs and schematics that can be interesting for the reader.

The first figure is a schematic of the ultrasonic immersion system (Figure B.1). The immersion system is an ULTRAPAC^{TM} system from NDT Automation, using UTWin software, together with an DPR300 pulser/receiver from JSR Ultrasonics.

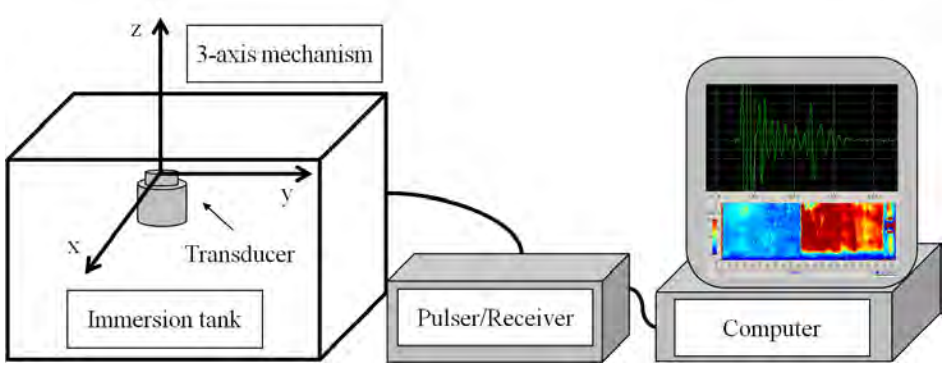

Figure B.1: A schematic of the ultrasonic testing system.

The two types of materials that were used for diffuse ultrasonic testing are seen in Figures B.2 and B.3.

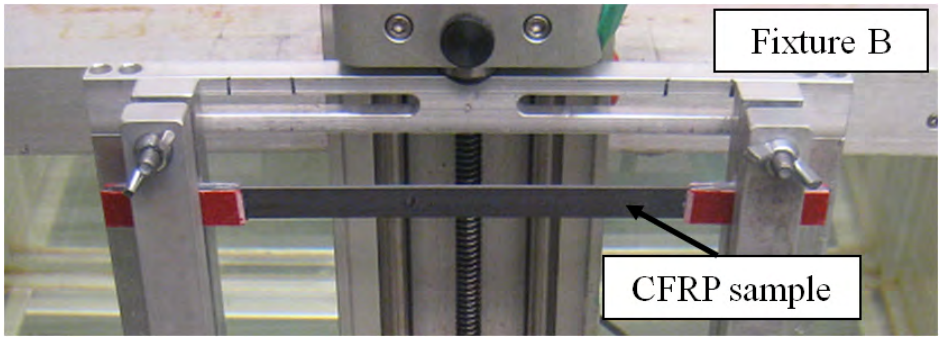

Figure B.2: One of the CFRP samples.

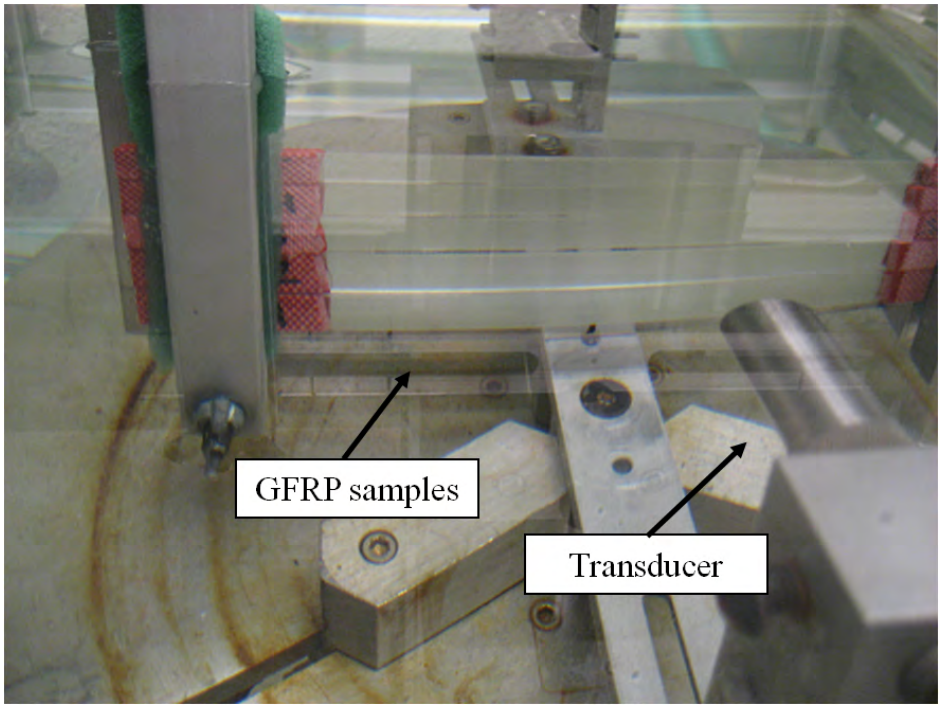

Figure B.3: GFRP samples.

The pulser/receiver can be set to pulse echo or through transmission set-up. Several parameters can be adjusted. The operator tries to adjust the parameter in such a way so the signal response is strong enough and gives a smooth response (see Figure B.4).

Figure B.4: Pulser/Receiver from JSR Ultrasonics.

Five samples of each material were used to determine the ultimate tensile strength. Most of the samples broked at the tabs. The tabs were ground in such a way so stress concentrations were minimized. But still the largest stress concentrations is at the tabs and therefore breakage is expected to be at the tabs. In Figure B.5 three photographs of broken samples can be seen. The first two samples have the most common failure morphology and the third one on the right hand side failed in a more peculiar way.

Figure B.5: Tensile test of the material used in experiments.

In Figure B.6 one can see how the set-up was done for all experiments. The last figure show how the transducers were adjusted for polar through transmission (Figure B.7). The proctractor was supposed to move with the fixture but it was later discovered that it did not move as expected. Therefore the angle of incidence in set-up D and E can differ by a few degrees.

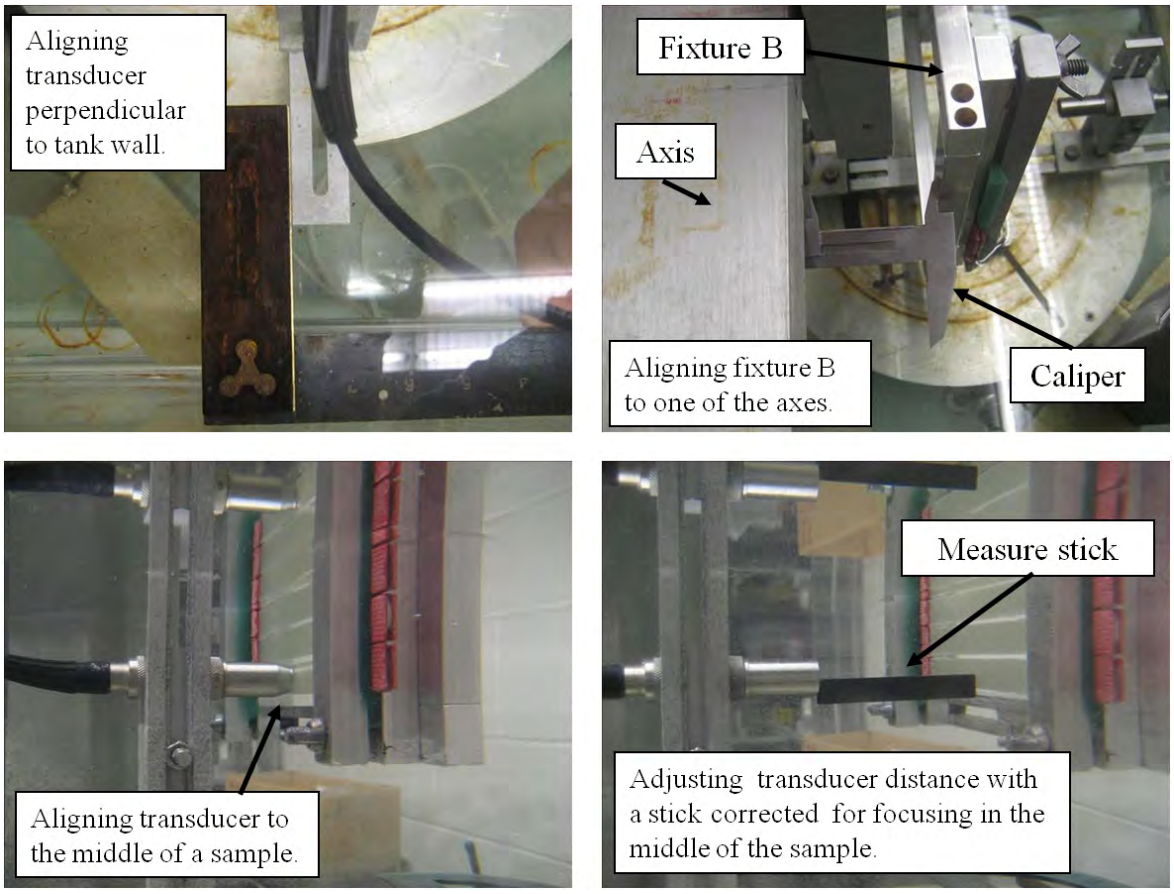

Figure B.6: Top left: Aligning transducer perpendicular to samples and tank wall, Top right: Aligning samples to axis, Bottom left: Centering transducer to sample, Bottom right: Applying the correct distance from sample.

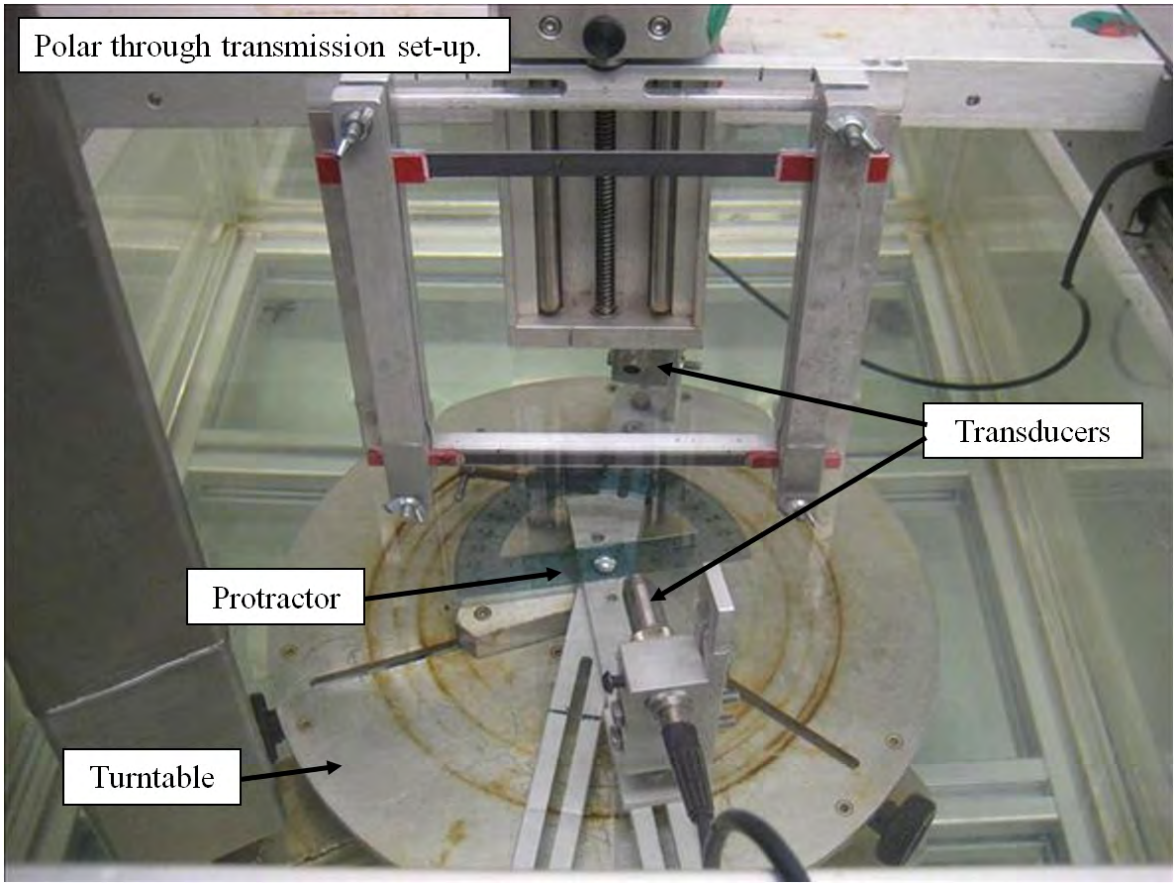

Figure B.7: Polar through transmission set-up where one can see the protractor.